



# Design of a facile, green and efficient graphene oxide-based electrochemical sensor for analysis of acetaminophen drug

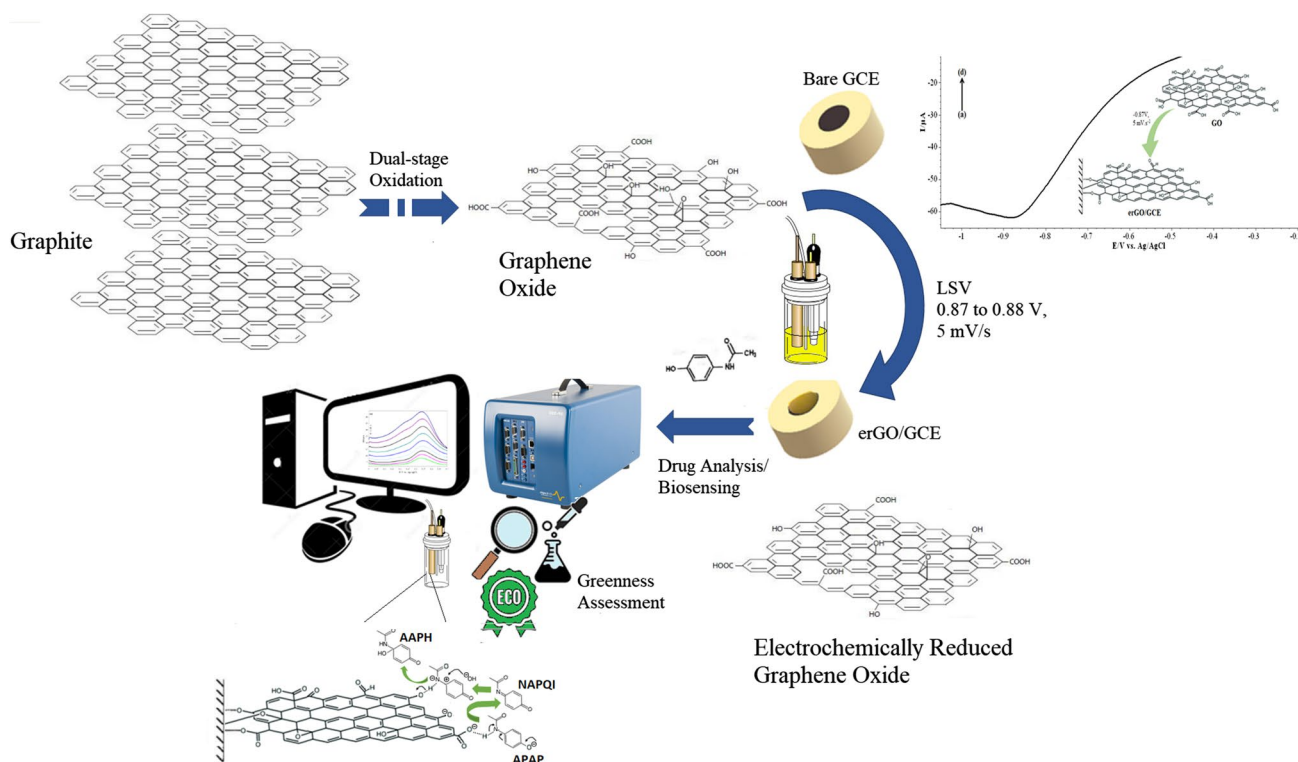
Muzamil Jalil Ahmed<sup>1</sup> · Shazia Perveen<sup>1</sup> · Syed Ghazanfar Hussain<sup>1</sup> · Arsalan Ahmed Khan<sup>1</sup> · Syed Muhammad Wahaj Ejaz<sup>1</sup> · Syed Muhammad Ali Rizvi<sup>1</sup>

Received: 30 July 2022 / Accepted: 10 December 2022 / Published online: 27 December 2022  
© Institute of Chemistry, Slovak Academy of Sciences 2022

## Abstract

In this study an efficient and environment friendly electrochemical sensor has been designed for the analysis of acetaminophen (APAP) drug. Electrochemical impedance spectroscopy, differential pulse voltammetry and cyclic voltammetric techniques were used to demonstrate the fabricated erGO/GCE sensor performance. Voltammetric assessment of acetaminophen drug was done using bare GC electrode, drop-casted GO/GC electrode and erGO/GCE electrochemical sensor. Proposed sensor was precisely validated for APAP detection by differential pulse voltammetric technique. Subsequently LOD, LOQ, sensitivity and linearity were determined and found to be 7.23 nM, 21.909 nM, 20.14  $\mu\text{A nM}^{-1} \text{cm}^{-2}$  and 0.0219–2.30  $\mu\text{M}$ , respectively. The diffusion coefficient of APAP was determined by chronoamperometry, and it was found to be  $2.24 \times 10^{-5} \text{cm}^2 \cdot \text{s}^{-1}$ . The synthetic and analytical steps were assessed as per the Green Chemistry's 12 Principles giving a 66 score (acceptable) and 93 score (excellent) for the said steps, respectively.

## Graphical abstract



**Keywords** Electrochemical sensors · Electrochemically reduced graphene oxide · Attenuated transmission resonance characterization · Acetaminophen · Analytical eco-scale assessment

### List of symbols

APAP	Acetaminophen/Paracetamol
ATR	Attenuated Transmission Resonance
<i>b</i>	Calibration curve slope
C or [...]	Concentration, M (mol L <sup>-1</sup> ) or μM (10 <sup>-6</sup> mol L <sup>-1</sup> )
Camp	Chronoamperometry
CV	Cyclic Voltammetry
ME	Modified Electrode
CPE	Constant Phase Element
D	Diffusion Coefficient (cm <sup>2</sup> s <sup>-1</sup> )
DPV	Differential Pulse Voltammetry
ECSA	Electrochemically (Active) Surface Area, (cm <sup>2</sup> )
ECME	Electrochemically Modified Electrode
EEC	Equivalent Electronic Circuit
erGO	Electrochemically Reduced Graphene Oxide
F	Faraday's Constant, 96,500 C mol <sup>-1</sup>
FWHM	Full-Width Height Maximum, viz. Warren Factor
GCE	Glassy Carbon Electrode
GME	Graphenic Modified Electrodes
GO	Graphene Oxide
GO/GCE	Graphene Oxide (over) Glassy Carbon Electrode
<i>i</i>	Measured Current (mA or μA)
<i>J</i>	Current Density, mA cm <sup>-2</sup> . Not to be confused with ' <i>j</i> = √- <i>I</i> ' in electrochemistry
<i>k</i>	Particle Shape Constant
LDA	L-DOPA, Levodopa, 3,4-dihydroxy-l-phenylalanine
LOD	Limit of Detection (nM)
LOL	Limit of Linearity (nM)
LOQ	Limit of Quantification (nM)
LSV	Linear Sweep Voltammetry
MDL	Measurable Detection Limit (nM or μM)
ME	Modified Electrode
<i>n</i>	Quantity (electrons, order etc.)
NAPQI	N-acetyl-p-benzoquinone imine
(P-)EIS	(Potentiostatic) Electrical Impedance Spectroscopy
QC	Quality Control
<i>R</i>	Universal Gas Constant, 8.314 J mol <sup>-1</sup> K <sup>-1</sup>
<i>R<sub>f</sub></i>	Roughness Factor
SD <sub>yx</sub>	Residual Standard Deviation
S/N	Signal-to-Noise Ratio
<i>v</i>	Scan rate, mV s <sup>-1</sup>

### Introduction

Graphene derivatives are well-known for their efficient electron-charge transfer, low current density (higher surface area) and remarkable electrocatalytic characteristics. These nanomaterials usually possess a general 2D honeycomb-like configuration of 1:3 sp<sup>2</sup>-hybridized carbon atoms arranged in a thin monolayer decorated with variable degree of oxygen-bearing hydroxyl, carbonyl, carboxylic and epoxy groups. Graphene derivatives like: graphene oxide (GO), and chemically reduced graphene oxide (rGO) or electrochemically reduced graphene oxide (erGO), have been used for various applications particularly in nanofiltration (Zhang and Chung 2017) drug delivery (Liu et al 2013), in the formulation of SARS-CoV-2 anaphylaxis vaccine (Cui et al 2020), and for energy storage (Pareek et al 2019). Furthermore, these nanomaterials have also gained much interest in their use as molecular recognition units and immobilization platforms in Modified Electrode (ME) designs for pharmaceutical, biotechnological and fast-moving consumer goods (FMCG) biosensing applications (Chen & Chatterjee 2013).

Acetaminophen (APAP, N-acetyl-p-aminophenol) is a common analgesic and febrifuge (anti-pyretic) (Ahmad J. 2011; James et al 2003). It can cause hepatotoxicity at doses higher than recommended levels due to the formation of NAPQI (N-acetyl-p-benzoquinone imine) by microsomal CYP<sub>450</sub> enzymes (Bessems and Vermeulen 2001). A facile, rapid, eco-friendly, sensitive and accurate analysis is required for APAP determination in pharmaceutical formulations and bioavailability assays. Titrimetry (Kumar and Letha 1997; Burgot G. et al. 1997), spectrophotometry (Moreira et al 2005; Nagaraja et al 1998), HPLC (Calinescu et al 2012; Ravishankar et al. 1998; Fujino et al 2005), colorimetry (Shihana et al 2010) and chemi-luminescence (Easwaramoorthy et al 2001) techniques have been developed for APAP determination. However, these methods involve extensive extraction prior detection and are impractical with regard to time management involved in QC testing. By contrast, electroanalytical techniques are versatile, rapid and highly sensitive, require relatively simple instrumentation and are moderate to low cost (Chen and Chatterjee 2013). The detection and quantification of APAP with acceptable precision and accuracy can viably be achieved by exploring their electroactive characteristics (Manjunathaa et al. 2011; Lu et al 2012; Liu G.T. et al. 2014; Kang et al 2010; Fan et al 2011; Patil et al 2019; Goyal et al. 2006; Chen X. et al. 2012; Babaei et al 2013). Electrochemically modified electrodes (ECMEs) exhibit controllable resistivity, high chemical

functionalization and electro-catalysis (Yu and Kim 2017), contributing to the advancement of electrochemical sensor varieties.

The fabrication of graphenic modified electrodes (GMEs) as bio- or rather electrochemical sensing platforms requires the synthesis of pristine GO nanosheets. The conventional syntheses for Graphene Oxide (GO) nanosheets as reported by Hummers and Offeman (1958), uses highly potent oxidants and corrosive acids. Later, some modifications in these syntheses have been attempted which were based on the ‘Tours method’ (Marcano et al 2010; Ahmad K. et al. 2018), but these syntheses still rely on expensive and often hazardous co-oxidants. More specifically, each of these methods results in significant defects which manifest as holes and gaps in the chemical structure of the graphene precursor. Furthermore, each of these methods employs the use of a relatively energy- and time-intensive syntheses and generates toxic pollutant  $\text{NO}_x$  gases such as  $\text{NO}_2$ ,  $\text{NO}$  and  $\text{N}_2\text{O}_4$ , whereas rGO synthesis can be chemical or electrochemical, the latter being much more efficient, green and more economical, whereas the former one employs significantly carcinogenic, highly corrosive and expensive reductants such as hydrazine hydrate (Stankovich et al 2007), hydriodic acid ( $\text{HI}$ ) and trifluoroacetic ( $\text{CF}_3\text{COOH}$ ) acid (Eigler and Hirsch 2012), and sodium borohydride (Khan Q.A et al. 2017) that can contaminate the final product. Chemical reduction, in frequent cases, fails to completely restore the defects developed in the structure and impedes the electrochemical, thermal and mechanical capabilities of the nanomaterial. It subsequently induces a detrimental reduction in the electron-charge transfer of the chemically modified electrodes (CMEs). Electrochemical reduction or electro-deposition is a rapidly growing nanoparticle surface immobilization technique, to fabricate electrochemically modified electrodes (ECMEs) allowing for better electro-catalytic properties necessary for electrochemical sensing (Yu and Kim. 2017; Yan et al. 2020). In contrast to electro-deposition, chemical reduction over substrate surfaces is significantly costly, hazardous, tedious, inefficient and complicated method that gives deposited nanomaterials of poor surface activity, defects and damaged morphologies that are unable to exploit their full potential for drug analysis and electrochemical sensing.

It is also significant for material chemists to consider the 12 Principles of Green Chemistry (DeVierno Kruder et al. 2017). The “green character” of synthetic and analytical procedures must be assessed and controlled via employing metrics, such as the green chemistry metrics (GCM) and Eco-scale (ES) for synthetic procedures, and Analytical Eco-Scale (AES), Green Analytical Procedure Index (GAPI) and Analytical Greenness Metric (AGREE) (Van Aken et al. 2006; Gałuszka et al. 2012; Sajid M. et al. 2022). An ‘ideal’ green analytical method must possess the following

qualities: (1) reagents are not hazardous; (2)  $< 0.1$  kWh per sample energy consumption; and (3) no waste generated.

Given this, herein, we report a time-efficient, less waste-effluent producing modification to the Tours’ Method for GO synthesis. We also demonstrate an optimized approach for obtaining rGO-deposited substrates from the prepared GO aqueous dispersion, by electrochemical means using linear sweep voltammetry. We also herein report the successful DPV-based voltammetric assay of the said fabricated electrochemical sensor, i.e. erGO/GCE for the detection of acetaminophen (APAP) at pH 1.0, which has not been studied previously. This work also presents the ES and AES approach to assess the greenness of proposed synthetic and analytical method. These two methods are simple, inexpensive, user-friendly, robust, comprehensive and broadly applicable metrics that cover a process and product specification based on accepted general industrial practices and allow considering vital sustainability alternatives.

## Material and methods

### Materials

Potassium permanganate ( $\text{KMnO}_4$ ), potassium nitrate ( $\text{KNO}_3$ ), 96–98% w/v sulfuric acid ( $\text{H}_2\text{SO}_4$  conc.), 30% v/v hydrogen peroxide ( $\text{H}_2\text{O}_2$ ), potassium hexacyanoferrate (III) ( $\text{K}_3[\text{Fe}(\text{CN})_6]$ ), reagent-grade sodium chloride ( $\text{NaCl}$ ) were prepared. 0.1 M HCl solution was prepared from 37% w/v hydrochloric acid, purchased from Merck (Darmstadt, Germany). Graphite powder (GP;  $\leq 98\%$  carbon,  $< 20$   $\mu\text{m}$  size, fine), uric acid (UA), ascorbic acid (AA) and levodopa (LDA) were purchased from Sigma-Aldrich (St. Louis, USA). HPLC-grade deionized (DI) water was purchased from Carlo-Erba (La Vaudreuil, France). All solutions were prepared using DI water throughout the course of our work. Drug sample solution was also prepared using 500 mg Panadol tablet (acetaminophen, GSK) in 0.1 M  $\text{HCl}_{(\text{aq})}$  (pH 1.0) for electrochemical analysis. This tablet was purchased locally.

### Instrumentation and methodology

#### Synthesis of graphene oxide (GO)

Graphene Oxide (GO) nanosheets were synthesized from a modified Tours’ method reported by Chen J. and co-workers (2013). Briefly, 0.5 g fine bulk graphite powder (1–3  $\mu\text{m}$  flakes,  $< 99.9\%$  C) was added to 12 mL concentrated  $\text{H}_2\text{SO}_4$  (96–98%) resulting in a black-coloured graphite-acid slurry. After vigorous agitation for at least 3 h, 1.0 g  $\text{KMnO}_4$  (99%) was added at a slow rate of  $100 \text{ mg} \cdot \text{min}^{-1}$  to limit the suspension temperature from exceeding 15–20 °C. A

quench system was used using a bath of ice-water slurry. It is possible to remove the ice bath after > 20 min of reaction time as the temperature remains fairly constant within the desired range. Successively, the reaction system is to be gradually heated for the next oxidation and was, thus, transferred to a 40 °C paraffin oil bath and vigorously stirred (at 120–150 rpm) for at least 30 min. Subsequently, the reaction mixture was diluted with 25 mL deionized water, followed by further stirring for 15 min at 95 °C. Additional dilution by 80 mL deionized water was followed by the slow addition of 2.5 mL 30% H<sub>2</sub>O<sub>2</sub>, turning the colour from dark-brown graphite oxide suspension to a golden–yellow colour, reminiscent of a GO aqueous dispersion. The overall graphite to oxidizer ratio is 1:2 by weight. The graphite oxide suspension (or supernatant) was transferred to a paraffin oil bath at 40 °C and heated for 2–3 h with vigorous agitation. Then, over the course of 15 min, 10 mL of the 30% H<sub>2</sub>O<sub>2</sub> was added at a specific reasonable rate at 95 °C with vigorous agitation to reduce the residual SO<sub>4</sub><sup>2-</sup>, MnO<sub>4</sub><sup>-</sup> and MnO<sub>2</sub> to colourless soluble MnSO<sub>4</sub>. The mixture was filtered and washed with 40 mL deionized water to remove the traces of MnSO<sub>4</sub> ions. The resulting solid was air-dried and diluted with 300 mL deionized water to give a graphite oxide aqueous dispersion which was stirred normally for 3–4 h. The graphite oxide aqueous dispersion was exfoliated to GO by ultra-sonication for 15–30 min using a 40 kHz Faithful FSF-010S Ultrasonic Cleaner (Hebei, China). The supernatant was then further centrifuged at 3000 rpm for 40 min, using Scilogex SCI412S Centrifuge (Connecticut, USA), to remove the unexfoliated graphite oxide. The GO aqueous dispersion was filtered, and the residue was air-dried. Alternatively, the supernatant suspension was not preheated but simply centrifuged at 1200 rpm for 15 min. The GO precipitate was then washed with deionized water several times to remove sulphate ions and trace Mn<sup>2+</sup> metal ions. The filtrate was dried in vacuum in a N<sub>2</sub> atmosphere at 60 °C for 5–6 h to obtain a dry crystallite solid.

### Fabrication of GO-based modified electrodes (MEs)

**GO/GCE ME Fabrication:** The GO/GCE electrochemical sensor was prepared by drop-casting method using GO<sub>(aq)</sub> suspension prepared earlier. Prior to the drop-casting, the GCE was carefully polished with 0.5 μm alumina powder slurry and rinsed thoroughly with DI water several times.

**erGO/GCE ME Fabrication:** To prepare 1:1 GO/NaCl<sub>(aq)</sub> dispersion, GO<sub>(aq)</sub> suspension was sonicated for 10–15 min and then mixed in equivalent amounts with 0.25 M NaCl<sub>(aq)</sub> solution to obtain a homogenous golden-yellowish dispersion. Alternatively, a 1 mg/mL GO/NaCl<sub>(aq)</sub> dispersion can also be prepared by mixing 250 mg of the GO crystallites with 250 mL of NaCl<sub>(aq)</sub> solution. The erGO/GCE electrochemical sensor was prepared by an optimized linear sweep

voltammetric (LSV) technique to improve deposition. Prior to the electrochemical fabrication, the GCE was carefully polished with 0.5 μm alumina powder slurry and rinsed thoroughly with DI water several times. LSV experiment was performed from 0.0 to –1.4 V potential, at a slow scan rate of 5 mV.s<sup>-1</sup>, in a nitrogen atmosphere using conventional three-electrode electrochemical cell. The electrochemical cell assembly comprised of a bare polished GCE over which the GO was reduced electrochemically, an Ag/AgCl reference electrode and a platinum wire counter electrode. LSV was performed using the Biologic SP-200 Potentiostat (Seyssinet-Pariset, France) with EC-Lab v11.10 Software. Each of these electrodes was distanced at least 5 mm from one another. The electrochemical reduction method produces uniform thin films of erGO over various substrates, possessing high electrocatalytic and electrochemical properties suited for use in electrochemical sensing applications.

### Characterizations

UV–Vis absorbance spectra were measured using a Shimadzu 1800UVA Series spectrophotometer (Kyoto, Japan) equipped with L2D2 DT Lamp (operating range: 190 nm to 800 nm). Crystallographic properties were probed from XRD data measured using the Malvern Panalytical X'Pert Pro X-Ray Diffractometer (Almelo, The Netherlands) equipped with Cu-anode tube as an X-ray source having wavelength of Cu/K<sub>α</sub> radiation of 10.154 nm. Chemical functionalization was probed by the FTIR technique using the Shimadzu FTIR-ATR Prestige IP-21 (Kyoto, Japan) equipped with attenuated total reflectance accessory. Morphological & surface texture was probed by FE-SEM technique performed using Joel JSM6380A (Tokyo, Japan) scanning electron microscope (operating limit: 30 keV and 10 mA). FE-SEM sample was coated with a thin layer of gold using a JEOL JFC-1500 sputterer (Tokyo, Japan) for 10–15 min under 0.1 atm.

Surface functionalization of the modified electrodes was probed by the ATR technique using the same instrument as that for the FTIR technique, with the exception that the attenuated total reflectance accessory consisted of a monolithic diamond ATR crystal and a flat, large width mechanical press for the particular experiment.

### Electroanalytical techniques

All electroanalytical techniques were performed using the Biologic SP-200 Potentiostat (Seyssinet-Pariset, France) with EC-Lab v11.10 Software, with the exception of Potentiostatic Electrochemical Impedance Spectroscopy (PEIS), which was performed using the CHI660E Electrochemical Workstation (Austin, Texas, USA). The conventional three-electrode electrochemical cell assembly

consisted of an Ag/AgCl (KCl saturated) as the reference and a platinum wire as the counter electrode. The working electrodes were the glassy carbon electrode (GCE; I.D.: 1.6 mm), the drop-casted graphene oxide modified GCE (i.e. GO/GCE), and the fabricated electrochemically reduced graphene oxide modified GCE (i.e. erGO/GCE). All measurements were taken against reference electrode. Experiment involving negative potential ranges was subjected to a 10–15-min  $N_2$  purging of the analyte solutions to remove dissolved  $O_2$ .

**Electrochemical performance evaluation of GO-based MEs.** The electrochemical behaviour and the charge-transfer characteristics of the fabricated GO/GCE and erGO/GCE were probed by recording CVs of the 5 mM  $K_4[Fe(CN)_6]_{(aq)}$  solution prepared in 0.1 M KCl. P-EIS analysis was performed using 5 mM  $Fe(CN)_6^{3-/4-}$  redox probe in 0.1 M  $KCl_{(aq)}$  by the conventional three-electrode cell, mentioned earlier. The experiment was performed from 10 mHz to 100 kHz at a constant potential of 0.1 V. EIS Spectral Analysis was performed by the EIS Spectrum Analyzer software (using amplitude-dependent algorithms).

**GO-based MEs sensing capabilities against (i) mixture of Levodopa (LDA), Uric acid (UA) and Ascorbic acid (AA) and (ii) Acetaminophen (APAP) tablet samples.** Based on the work of Yu and Kim (2017), electrochemical performance of the fabricated sensor was evaluated. A mixture of 50  $\mu$ M Levodopa (LDA), 10  $\mu$ M Uric Acid (UA) and 1 mM Ascorbic Acid (AA) was prepared in 0.1 M PBS (pH 7.0), and voltammograms were recorded using DPV and CV techniques. Differential pulse voltammograms of mixture were recorded in the potential window of  $-0.2$  to  $0.5$  V, at 25 mV/s scan rate. An optimized performance was observed when pulse height ( $P_H$ ), pulse width ( $P_W$ ), step height ( $S_H$ ) and step time ( $S_T$ ) were set as 100 mV, 100 mS, 10 mV, 400 ms, respectively.

The fabricated erGO/GCE was also employed for probing cyclic voltammetric response of a solution of 0.1 M (20 mg/mL) APAP in 0.1 M HCl (pH 1.0) in the potential window of  $-0.4$  to  $1.2$  V at 30 and 50 mV/s scan rates. Furthermore, differential pulse voltammograms of APAP samples were also recorded at various concentration (0.1, 0.2, 0.3, 0.4, 0.7, 0.9, 2.3, 4.7 and 23  $\mu$ M) using fabricated erGO/GCE electrochemical sensor. The DPV was performed at a potential range of 0.0 to 0.5 V at 8 mV.s $^{-1}$  scan rate. An optimized performance was observed using the following set of conditions for the DPV, where pulse height ( $P_H$ ), pulse width ( $P_W$ ), step height ( $S_H$ ) and step time ( $S_T$ ) were set as 100 mV, 200 mS, 4 mV, 500 ms, respectively. CAmp was also used to investigate the amperometric response for the APAP samples having concentrations 0.1  $\mu$ M, 0.2  $\mu$ M, 0.4  $\mu$ M, 0.5  $\mu$ M, 0.7  $\mu$ M, 0.9  $\mu$ M, respectively, at a fixed potential of 0.35 V (APAP electro-oxidation potential).

## Results and Discussion

### Characterization of the synthesized graphene oxide (GO) nanosheets

#### UV–Vis spectroscopy

UV–Vis spectroscopy is a useful technique for identification and quantification of chemical compounds. Figure 1A shows a maximum absorbance at 228 nm wavelength. This UV–Vis absorbance value is attributed to the  $\pi$ – $\pi^*$  transitions of the aromatic C–C bond in the GO lattice (Veerapandian et al 2012; Song et al 2014; Eigler and Dimiev 2016). In comparison of this, UV–visible spectra of graphite starting material have also been recorded and the maximum absorbance of the commercial graphite powder was found at 271 nm wavelength, similar to the literature value (Senthil et al 2017). UV–Vis absorbance is proportional to the population of a significant functional group within the characteristic  $sp^2$ -conjugated domains in the graphene carbon lattice. This absorbance in turn is related to a significant retention of the characteristic carbon lattice of graphene after the multi-stage oxidation steps. Additionally, a small shoulder peak at around 298.7 nm is due to the  $n$ – $\pi^*$  transitions of the C=O bond (Hidayah et al 2017). This absorbance is related to an increase in the relative number of C=O bearing groups with respect to the  $sp^2$ -conjugated domains.

#### X-ray diffraction

X-ray powder diffraction (XRD) is a rapid analytical technique primarily used for phase identification of a crystalline material and can provide information on unit cell dimensions. The analysed material is finely ground, homogenized, and average bulk composition is determined (GO graphene; Dorset 1998). Figure 1B shows a representative XRD spectrum of a finely ground, homogenized powder of the ‘as-prepared’ GO nanosheets.

Data of the XRD spectra are tabulated in Table 1. The XRD pattern shows the two narrow peaks arising from (002) and (010) reflection from the crystalline planes, giving  $2\theta^\circ$  values of  $10.03^\circ$  and  $41.12^\circ$ , respectively. The narrow peak reflections can be attributed to the relatively small size of the GO nanosheets. Note that the (002) reflection peak refers to the crystalline plane that is perpendicular to the plane of GO showing the  $d$ -spacing. The (010) reflection peak refers to the crystalline plane that is parallel to the plane of GO showing the  $d$ -spacing. Moreover, the interlayer spacing ‘ $d$ ’ between the GO layers was calculated to be 0.86 nm and 2.14 nm for the (002) and (010) reflections, respectively, using Bragg’s law (Eq. 1) (Veerapandian et al 2012; Hidayah et al 2017).



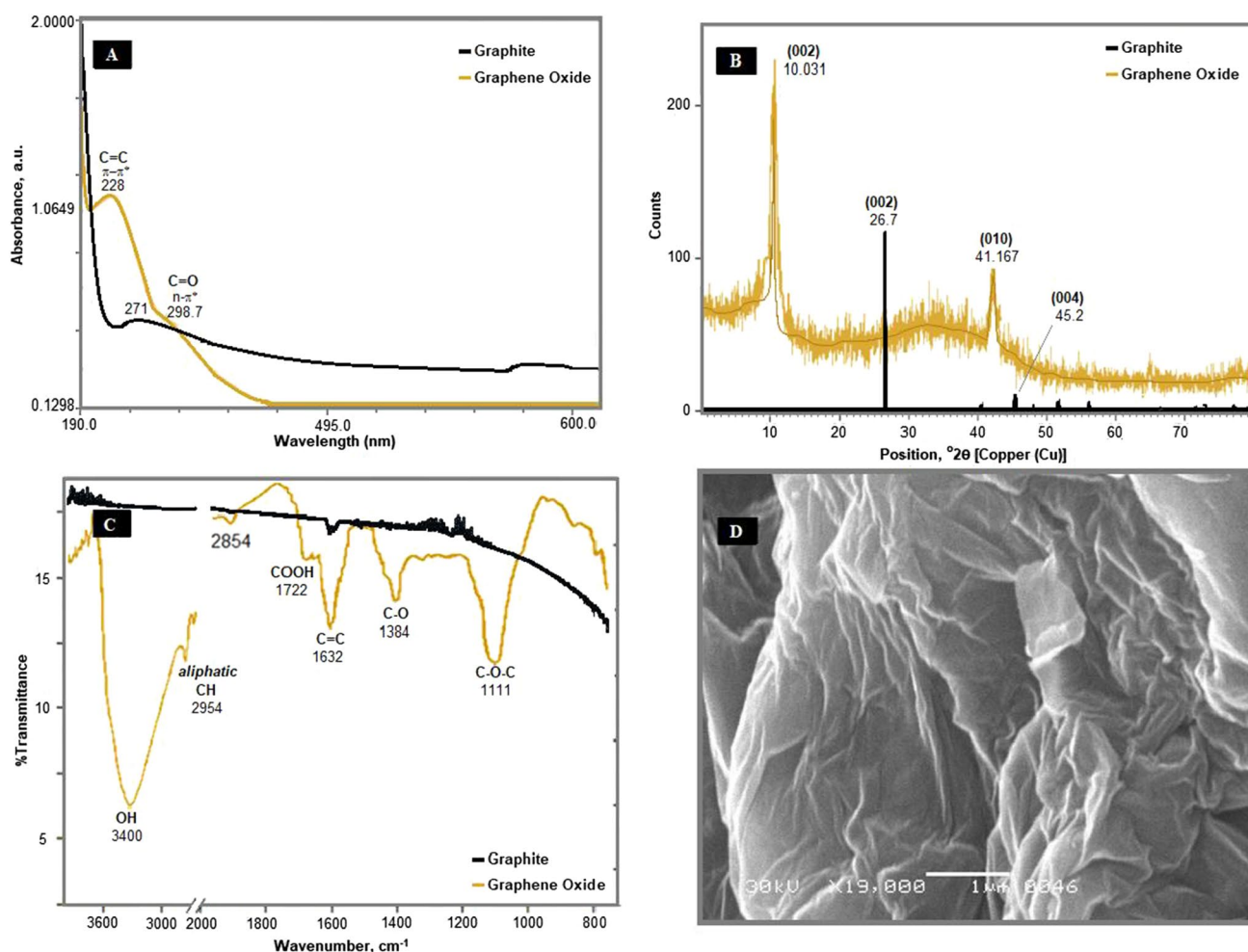


**Fig. 1** Characterization of the ‘as-prepared’ GO and the graphite powder using: **A** UV–Vis spectra, **B** XRD, **C** FTIR. **D** FE-SEM for ‘as-prepared’ GO crystallites (19,000x, 1  $\mu\text{m}$ , 30 kV)

**Table 1** XRD result of the synthesized GO crystallites

Miller index	$2\theta^\circ$	FWHM ( $2\theta^\circ$ )	$d$ (nm)	$\tau$ (nm)
(002) (H)	10.031	1.443	0.858	26.5
(010) (D)	41.167	0.590	2.144	4.5

where ‘ $2\theta^\circ$ ’ is the diffraction angles; ‘FWHM’ is the full-width height maximum (aka the Warren factor); ‘ $d$ ’ is the d-spacing, ‘ $\tau$ ’ is the mean size of the 2D nanosheets of diameter/width ‘ $D$ ’ and height ‘ $H$ ’

$$n\lambda_{\text{Cu}/K\alpha} = 2d\sin(\theta); \quad (1)$$

where ‘ $n$ ’ is the order of diffraction that is determined by the diffractometer. The ‘ $d$ ’ spacing is proportional to the degree of oxidation. The calculated ‘ $d$ ’ spacing from the XRD data corresponding to (002) reflection for the GO, is relatively higher than that reported in the literature to date (Veerapandian et al 2012; Hidayah et al 2017). This implies an extremely higher degree of oxidation, which in turn

validates the efficiency of the improved synthesis of GO. Furthermore, the relative mean size ‘ $\tau$ ’ was also calculated from the full-width height maximum ‘FWHM’ values of 1.44 and 0.59 for the (002) and (010) reflections. The reflection (002) gives the average height ‘ $H$ ’ and (010) gives the average diameter ‘ $D$ ’ of the GO crystallite created according to an embodiment method of the present invention. The mean size was determined to be 26.5 nm  $\times$  5.5 nm, using the Debye–Scherrer equation (Eq. 2) (Dorset 1998):

$$\tau = \frac{k\lambda_{\text{Cu}/K\alpha}}{(\text{FWHM})\cos(\theta)}; \quad (2)$$

where the shape factor ‘ $k$ ’ is assumed to be 0.89 for spherical crystals possessing a cubic symmetry (Dorset 1998).

A high FWHM value for the (002) reflection implies that the GO crystallites were abundant in that particular crystallographic arrangement. It can be noticed from Table 1 that FWHM values are proportional to the particle size. The

reflection peaks are particularly narrow and sharp which further validates the efficiency of our method and its suitability to synthesize GO nanosheet flakes with sizes in the nanoscale. The presence of defects is manifested by broader peaks. Our XRD results show sharp reflections, suggesting GO nanosheet flakes are formed with low defects in its structure and thereby further support the effectiveness of the modified method of GO synthesis.

When XRD spectra of commercial graphite powder were recorded, an extremely sharp (002) reflection was noticed at  $26.7^\circ$  as well as a small (004) reflection was observed at  $45.2^\circ$ . These are attributed to the graphite structure with *d*-spacing of 0.335 nm, consistent with the literature (Low et al 2015; Popova 2017; Hidayah et al 2017).

### FTIR spectroscopy

FTIR detection can be a very useful tool in identification of functional groups and unknown compounds. The major functional groups identified from Fig. 1C, in the ‘as-prepared’ GO nanosheet crystallites, include: a broad C–OH stretching band centred at  $3402\text{ cm}^{-1}$  due to absorbed moisture by the porous-like GO crystallite. The peak broadening observed in Fig. 1C is attributed to the C–OH $\cdots$ H bonding interaction due to the adsorption of moisture on the porous-like GO surface, as reported in various literature (Veerapandian et al 2012; Hidayah et al 2017). Further, the peak at  $2925\text{ cm}^{-1}$  is characteristic of aliphatic C–H ( $\text{sp}^3$  carbons) and a shoulder at  $2854\text{ cm}^{-1}$  generally reported in the literature to be associated with aldehydic C–H group. Moreover, groups identified include: a symmetric C=O stretching peaks at  $1722\text{ cm}^{-1}$ , a sharp and strong absorption at  $1632\text{ cm}^{-1}$  of C=C bonds, C–O vibration and C–O–C (epoxide) vibration at  $1384\text{ cm}^{-1}$  and  $1111\text{ cm}^{-1}$ . Thus, the observed spectral peak positions are in very good agreement with reported literature on graphene oxide (Veerapandian et al 2012; Chen J. et al. 2013; Song et al 2014; Eigler & Dimiev 2016; Hidayah et al 2017; GO graphene). In the course of this, a comparison study between the FTIR spectra of the GO and the initial graphite has also been done. The typical C=C stretching band of graphite is observed around  $1632\text{ cm}^{-1}$ , consistent with the literature (Senthil et al 2017). Such findings imply the complete oxidation of the graphite to GO.

### Field emission scanning electron microscopy

Field emission scanning electron microscopy (FE-SEM) is an electron microscopic technique, employed to characterize the surface morphologies and roughness of a material. Figure 1D shows a FE-SEM image of a synthesized GO crystallite, revealing a typical 2D morphology of these crystallites. It can be noticed from figure that it comprises crumbled and folded textures, irregular edges, a few pores

and rough surface. The excess oxidation of graphite layers often results in the development of variably sized pores. The carbon lattice was ‘eaten away’ by the oxidizer, whereby released CO and CO<sub>2</sub> gases may propagate the pore formation process. Therefore, the approach of two steps oxidation has been adopted in this study.

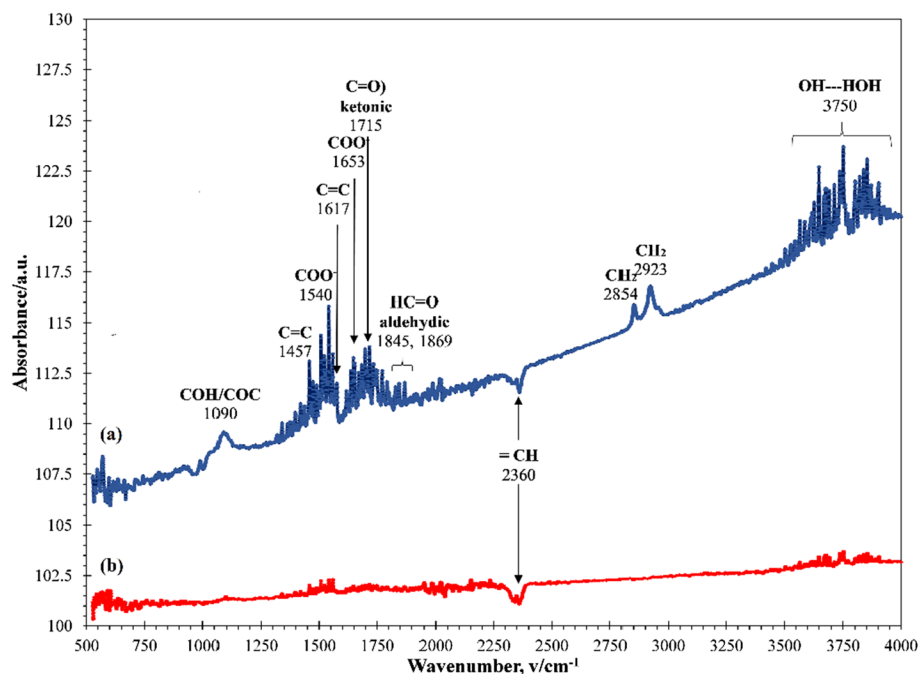
### Characterization of the fabricated sensors

#### Facile attenuated total reflection (ATR) characterization of an electrodeposited substrate

ATR spectra of bare glassy carbon electrode (i.e. the GCE) and electrochemically reduced graphene oxide deposited on the GC electrode (i.e. the erGO/GCE) have been recorded to study the surface functionalization. Figure 2(b) shows the ATR spectra of bare GCE, where the peaks characteristic to the C=C bonds at  $1617\text{ cm}^{-1}$  and alkenic =CH stretching peaks at  $2630\text{ cm}^{-1}$  were found to appear. No additional significant peaks were observed for the bare GCE. More recent research has also suggested that the glassy carbon is 100%  $\text{sp}^2$ , possessing a flattened fullerene-like structure (Harris 2004), whereas Fig. 2(a) shows the ATR spectra of the thin-film deposited substrate i.e. erGO/GCE. A significant number of symmetric stretching peaks associated with the oxygen-bearing functional groups appeared at this spectra indicating the presence of aldehydic group C=O peaks at  $1845\text{ cm}^{-1}$  and  $1869\text{ cm}^{-1}$ , carboxylic group C=O peak at  $1715\text{ cm}^{-1}$ , a ketonic group C=O peak at  $1653\text{ cm}^{-1}$  and an epoxide group C–O–C peak at  $1090\text{ cm}^{-1}$ .

The bending peaks of –COO, C–O–C and/or –C–OH groups at  $1540\text{ cm}^{-1}$  and  $1090\text{ cm}^{-1}$  are of considerable interest as they characterize the bonding interaction of the erGO nanosheet to the bare GCE. The observed values of transmittance are in good agreement with the literature (Tsai et al 2011; Mudunkotuwa et al 2014). The obvious difference in terms of transmittance intensity between the bare polished GCE and the erGO/GCE can be observed. The transmittance intensity is proportional to the degree of oxidation or simply, the population of oxygen bearing groups. This in turn relates to a more deflected infrared radiation for the latter due to presence of oxygen bearing groups on the GO  $\text{sp}^2$ -conjugated carbon lattice which transmit the incident infrared radiation more than the bare glassy carbon electrode. It is to be noted that no well-defined structural model exists for GO or erGO due to the random distribution of oxygen-bearing functional groups (Mudunkotuwa et al 2014). Although the chemical composition and structure of GO is still indistinct, it could be stated that hydroxyl, carboxyl and epoxy are amongst the leading groups with regard to points of interaction. Therefore, we propose two probable models of erGO interaction with GCE. These points of interaction are shown in Fig. 3.

**Fig. 2** ATR spectra of **a** erGO/GCE & **b** bare GCE



### Fabrication of the erGO/GCE electrochemical sensor by linear sweep voltammetry (LSV)

Figure 4A shows the linear sweep voltammogram (LSV) of  $1 \text{ mg}\cdot\text{mL}^{-1}$  GO/ $0.25 \text{ M}$  NaCl solution. To study fabrication of GO suspension on bare GCE, LSV was recorded at  $0.0 \text{ V}$  to  $-1.4 \text{ V}$  potential range. A considerably distinct broad peak at  $-0.87 \text{ V}$  was appeared which confirms the electrochemical reduction of GO on GCE. Furthermore, no appropriate response was observed at repeated scans implying most of the sites on the GCE surface are immobilized by GO nanosheets. The erGO/GCE fabrication was optimized at  $5 \text{ mV/s}$  scan rate comparatively to the work of Yu and Kim (2017) across varying scan rates ( $10$  to  $100 \text{ mV}\cdot\text{s}^{-1}$ ), as shown in Fig. 4B. A higher erGO thin-film electro-deposition/electro-reduction was observed with increased reaction time at slow scan rate. The electrodeposition/electro-reduction potential ( $-0.86 \pm 0.01 \text{ V}$ ) was found to be in good agreement with that reported in the literature (Yu and Kim 2017; Yan Q., et al. 2020).

### Electrochemical performance evaluation of GO-based MEs

The electrochemical characteristics of oxygenate graphenic nanomaterials such as GO and erGO is drastically effected by the textural, morphological properties which are subject to type of methods used to synthesize the said nanomaterials. The degree of oxidation also drastically impacts the  $\text{sp}^2$  bonding disruption, electrocatalytic behaviour and electrochemical performance of the said nanomaterials.

### Cyclic voltammetry (CV)

Cyclic voltammograms of  $5 \text{ mM}$   $[\text{Fe}(\text{CN})_6]^{3-}$  in  $0.1 \text{ M}$   $\text{KCl}_{(\text{aq})}$  solution were recorded using bare GCE and GO-based MEs (Fig. 5A). It can be noticed that erGO/GCE illustrates considerably well-defined redox character of this analyte as compared to GCE. Such as, exhibited peak potential difference,  $\Delta E_p$ , for GCE ( $138 \text{ mV}$ ) is higher

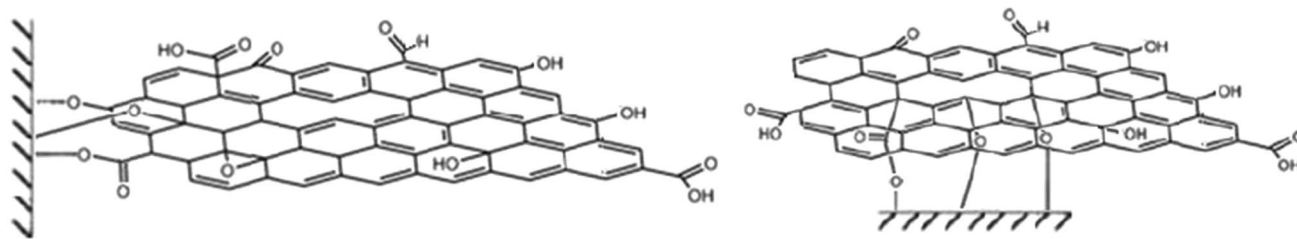


**Fig. 3** Proposed models of the points of interaction of the erGO nanosheets with the GCE interface



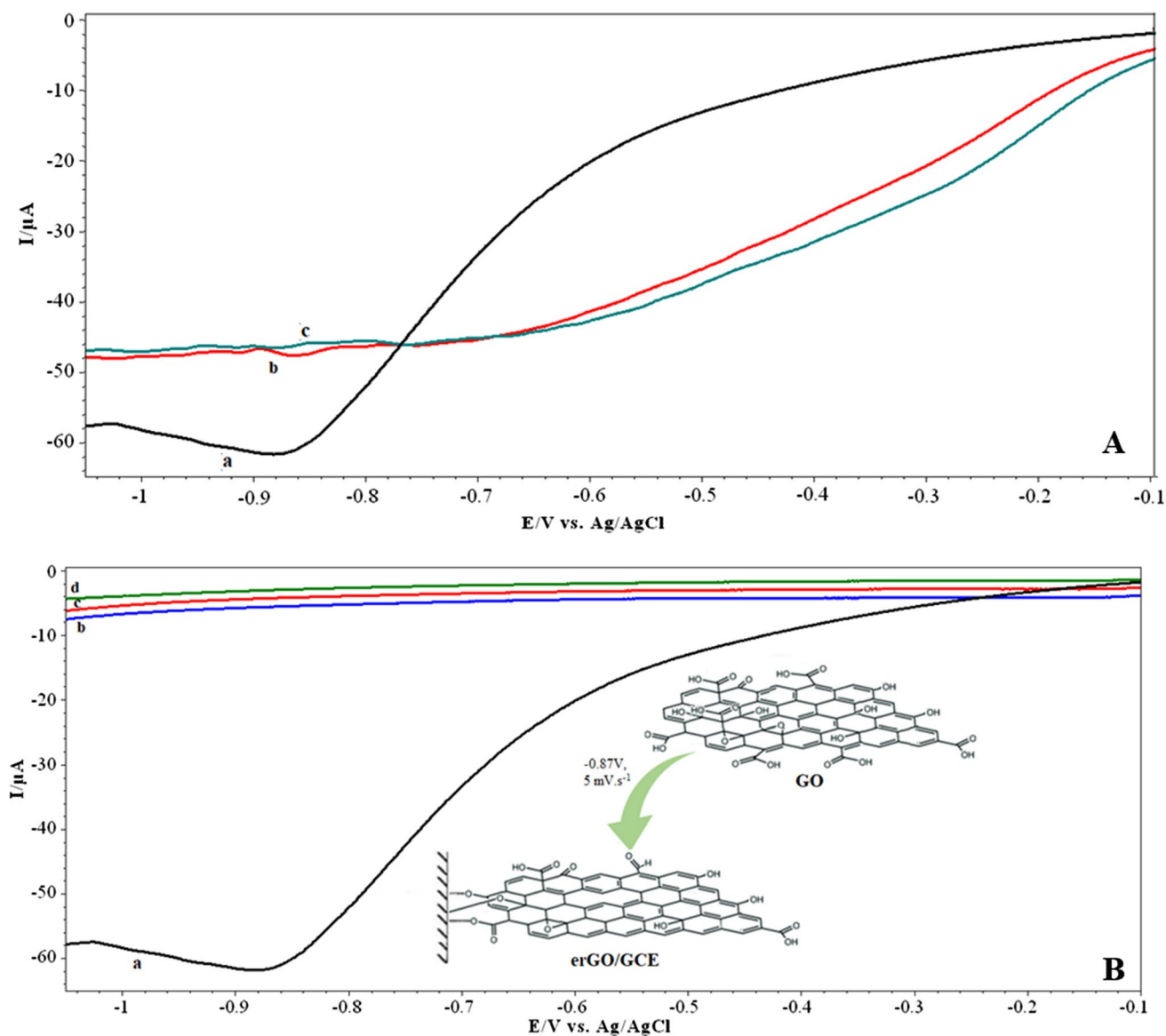


**Fig. 4** **A** Effect of repetitive LSV electrodeposition at constant scan rate of  $5 \text{ mV}\cdot\text{s}^{-1}$  for erGO/GCE fabrication where (a) 1st scan with electro-reduction at  $-0.87 \text{ V}$ , (b) 2nd scan with electro-reduction at  $-0.86 \text{ V}$ , and (c) 3rd scan (no response), whereas **B** illustrates

the effect of different LSV scan rates at (a) 5, (b) 10, (c) 50 and (d) 100  $\text{mV}\cdot\text{s}^{-1}$  for erGO/GCE fabrication. Inset: GO electro-reduction/electro-deposition reaction

than erGO/GCE (106 mV). Further to that, higher peak currents of this redox analyte were observed for the erGO/GCE, owing to the higher aspect ratio, surface activity and optimum current density, featured the excellent electrocatalytic behaviour of this sensor. A significant contrast is observed for the drop-casted GO/GCE with considerably lower peak currents and a larger peak potential difference (163 mV). It may be due to the abundant oxygen-bearing groups in that crystallites which induce stability effects leading to relatively higher resistivity (Yan Q. et al. 2020).

Results are compliant with reported values (Yu and Kim 2017). We, however, suspect the consequent differences are

due to the variable manufacturing practices for the Graphite Powder, used to prepare the GO and erGO nanosheets in our work. CV results are tabulated in Table 2.

#### Potentiostatic electrochemical impedance spectroscopy (P-EIS)

*Electrocatalytic behaviour and comparative performances.* Figure 5B shows the EIS-Nyquist spectra of erGO/GCE, GO/GCE and bare GCE. The semicircles observed correspond to charge transfer resistance ' $R_{ct}$ ' limiting phenomena at the solution–electrode interface associated with the

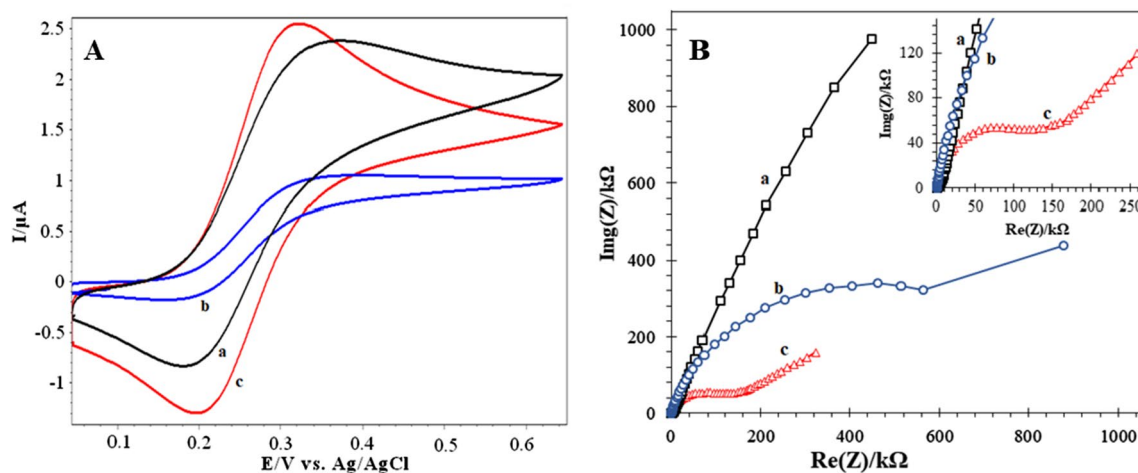


**Fig. 5** **A** Cyclic voltammogram measured from 0.0 V to 0.6 V at 10 mV/s scan rate, and **B** the Nyquist EIS spectra at an applied frequency of 10 mHz to 100 kHz, at 0.1 V; of 5 mM  $[\text{Fe}(\text{CN})_6]^{3-/4-}$  in

0.1 M  $\text{KCl}_{(\text{aq})}$  for (a) bare GCE, (b) drop-casted GO/GCE and (c) fabricated erGO/GCE

**Table 2** CV Peak Currents and Potentials of 5 mM  $[\text{Fe}(\text{CN})_6]^{3-/4-}$  in 0.1 M  $\text{KCl}_{(\text{aq})}$  solution at 10 mV/s, using (i) bare GCE, and (ii) drop-casted GO/GCE and (iii) fabricated erGO/GCE

#	Ratio*	Working electrode	Anodic		Cathodic		Peak separation* $\Delta E_p/\text{V}$	Current $i_{p,c}/i_{p,a}$
			$V_{p,a}/\text{V}$	$i_{p,a}/\mu\text{A}$	$V_{p,c}/\text{V}$	$i_{p,c}/\mu\text{A}$		
(i)		GCE	0.343	2.347	0.205	-0.767	0.138	0.327
(ii)		GO/GCE	0.343	1.009	0.170	-0.767	0.163	0.174
(iii)		erGO/GCE	0.311	2.529	0.205	-1.288	0.106	0.509

\*Calculations must not be confused with diagnostic tests which are valid for 20–50 mV/s scan rates only

system under analysis, whereas the straight line of slope approximately equal to 1.0, angled at  $45^\circ$ , corresponds to a diffusion-limited charge transfer phenomena at the solution–electrode interface. As evident, results indicate the charge-transfer resistance  $R_{ct}$  of the fabricated erGO/GCE which is found to be approximately half that of the bare GCE. A rapid electron transfer can be observed for the former, owing to its fairly high electrocatalytic property. It can be further evidenced from the results of the CV experiments using the standard redox probe. Conversely, the non-ideal ‘true’ capacitance, for erGO/GCE (98.71  $\mu\text{F}$ ), was much higher compared to the bare GCE (46.54  $\mu\text{F}$ ). The ‘true’ capacitance value corresponds to non-ideal capacitive behaviour that in turn has implication regarding surface irregularities and thickness of the deposited films of active materials, namely: GO and erGO. The high  $R_{ct}$  (831.81 k $\Omega$ ) and low C (43.82  $\mu\text{F}$ ) for GO/GCE imply high charge-transfer loss due to the higher degree of oxidation for GO which stabilizes the GO nanosheet and hinders free electron transfer. These findings were found to be similar as reported in the literature (Roy et al 2011; Casero et al 2012; Yu and Kim 2017). It is to be observed that the magnitude of the charge-transfer resistance for the GO is ca. 6 times higher than erGO. The charge transfer resistance is inversely related

to the capacitance, which in turn is related to the hindrance of electron transfer due to higher degree of oxidation, stabilization by conjugation of the  $\text{sp}^2$  carbons in the graphenic lattice as well as due to the presence of defects that may contribute to poor electrochemical performance.

**Equivalent electronic circuit (EEC) modelling.** The charge-transfer resistance ‘ $R_{ct}$ ’ of bare GCE, drop-casted GO/GCE and fabricated erGO/GCE was determined by fitting analysis of the EIS spectra as shown in Fig. 6 and Table 3. The impedance diagrams gave a ‘good’ fit with the proposed electrical equivalent circuits (EECs), as shown in Fig. 6(a–c). The fitting circuit for erGO/GCE and bare GCE is represented using a Randles-Warburg circuit with one Constant Phase Element [(Circuit Notation:  $R_s + Q_1/(W + R_{ct})$ ]. This EEC comprises: the electrolyte resistance ‘ $R_s$ ’, the charge transfer (or polarization) resistance ‘ $R_{ct}$ ’ and a constant phase element ( $Q_1$ ) simulating non-ideal capacitive behaviour due to surface irregularities and thickness of the deposited film. The combination of  $R_{ct}$  and  $Q_1$  models semi-infinite linear diffusion through an inhomogeneous glassy carbon surface or a partially oxidized graphene (erGO) nanosheet layer.

The Warburg element ‘W’ typically models the semi-infinite linear diffusion, i.e. the unrestricted diffusion to a

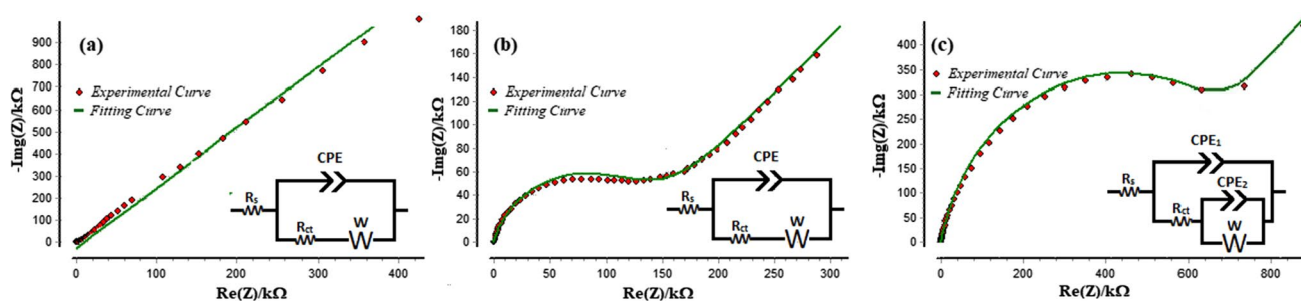


**Fig. 6** The corresponding fitting curves of the EIS-Nyquist spectra of **A** bare GCE, **B** drop-casted GO/GCE and **C** fabricated erGO/GCE. Inset: Corresponding EECs are also illustrated

**Table 3** EIS results and low estimated errors (%), evaluated after comparison with fitting data

	erGO/GCE		GO/GCE		GCE	
	Result	Error (%)	Result	Error (%)	Result	Error (%)
$\omega_{max}$ (rad.s <sup>-1</sup> )	45.92	–	7140.0	–	26,847.0	–
$R_s$ (kΩ)	0.32	3.86	0.37	3.5	0.68	2.14
$R_{ct}$ (kΩ)	135.06	3.03	831.81	2.98	311.65	2.99
$\sigma$ (Ω.s <sup>-1/2</sup> )	105.29	2.01	1615.5	1.13	54.66	5.43
$Q_1$ (μS.s <sup>n</sup> )	182.09	1.88	142.04	2.00	500.88	3.47
$Q_2$ (μS.s <sup>n</sup> )	–	–	71.89	1.87	–	–
$W$ (Ω.cm <sup>2</sup> )	21.98	–	27.04	–	0.39	–
$C$ (μF)	98.71	–	43.82	–	46.54	–
$n_1$	0.84	0.26	0.87	0.40	0.84	0.77
$n_2$	–	–	0.83	–	–	–

where ‘ $\omega_{max}$ ’ is the maximum angular frequency, ‘ $R_{ct}$ ’ is charge-transfer resistance, ‘ $R_s$ ’ is solution resistance, ‘ $\sigma$ ’ is Warburg coefficient, ‘ $Q_1$ ’ corresponds to CPE1 and CPE2 non-ideal capacitances, ‘ $C$ ’ is charge-transfer capacitance, ‘ $n_i$ ’ are exponents corresponding to CPE1 and CPE2 elements

large planar electrode. The fitting circuit for GO/GCE is represented using a Randles-Warburg circuit with two Constant Phase Elements [(Circuit Notation:  $R_s + Q_1/(Q_2/W) + R_{ct}$ )]. In addition to  $R_{ct}$  and  $Q_1$ , the  $Q_2$  and  $W$ , elements model finite-length diffusion through an inhomogeneous oxidized graphene (GO) nanosheet of finite length. In both the proposed EEC models, distributed elements are to be used instead of a capacitor, owing to the distribution of relaxation times as a consequence of surface irregularities. The CPE provides a good description of a solid–liquid interfacial behaviour, whereas the Warburg element is observed particularly for electrochemically modified electrodes (ECMEs) having reduced or oxidized graphene-based nanomaterials (Connor et al 2020).

The Warburg impedance can be calculated from the EIS data using Eq. 3. For an ‘ $n$ ’ exponent within the range of  $0.7 < n < 0.9$ , the behaviour of the active material deposited onto the electrode is said to be approximate of an ideal capacitor, i.e. the active material possesses high charge-transfer properties. The ‘ $n_1$ ’ or ‘ $n$ ’ exponent corresponds to the diffusion process (low frequency region) lies within the range of  $0.7 < n < 0.9$ ; then, CPE behaviour is close to that

of an ideal capacitor having a ‘true’ capacitance given by Eq. 4. Surface irregularity and charge-transfer loss due to film thickness and inhomogeneity is much more significant in chemically modified electrodes (CMEs) prepared by casting methods, as evident from the results.

$$W = |Z| = \sqrt{2} \left( \frac{\sigma}{\sqrt{\omega}} \right); \tag{3}$$

$$C = Q_1(\omega_{max})^{n-1}; \tag{4}$$

It was observed that erGO/GCE exhibited a lower charge-transfer resistance (135.06 kΩ) as compared to GO/GCE which exhibits an extremely high charge-transfer resistance (831.81 kΩ). Furthermore, the fitted EIS data also provide the ‘ $n$ ’ exponent values corresponding to the diffusion process (low-frequency region). It was found to be 0.87 for erGO/GCE and 0.84 for GO/GCE. The electrochemical process at the electrolyte–electrode interface for erGO/GCE and bare GCE (diffusion-limited systems) is illustrated in Fig. 7(a), whereas Fig. 7(b) corresponds the same for GO/

GCE (diffusion-controlled charge-transfer system). For GO/GCE, it can be noticed that the cathodic concentration gradient hinders the mass-transfer. Further to that, surface irregularities and degree of oxidation also contribute to a high charge-transfer loss and poorer capacitance.  $R_{ct}$  and  $CPE_1$  model the diffusion through the partially oxidized or unoxidized surfaces (here, erGO and GCE), while a combination of  $R_{ct}$ ,  $CPE_2$  and  $W$  models the diffusion through an oxidized surface of finite length.

**Determination of the electrochemically active surface area (ECSA) by EIS.** The electrochemically active surface area (ECSA) of the modified electrodes can also be determined from the EIS data, using Eq. 5. The specific capacitance ' $C_s$ ' describes the capacitance of an ideal flat surface of an immobilized material. For  $C_s$ , reported values lie in the range of 20–80  $\mu\text{F}/\text{cm}^2$  (Connor et al 2020); however, the average value of 40  $\mu\text{F}/\text{cm}^2$  as reported in the literature has been used (Selvam et al 2020). Furthermore, the roughness factor ( $R_f$ ) can also be determined by Eq. 6 (Casero et al 2012). With GCE (1.6 mm dia) surface area is 0.283  $\text{cm}^2$ . More so, the exchange current densities ( $J_{WE}$ ) can also be determined from the EIS data using Eq. 7 (Connor et al 2020) for an ' $n$ '-electron-transfer redox event at 25 °C. Estimated values are tabulated in Table 4.

$$\text{ECSA} = C/C_s; \quad (5)$$

$$R_f = \frac{A_{WE}}{A_{GCE}}; \quad (6)$$

$$J_{WE} = \frac{RT}{nFR_{ct}} = \frac{0.0257}{R_{ct}} \left( \frac{A}{\text{cm}^2} \right) \quad (7)$$

GO is not conductive due to the abundance of oxygen-bearing groups that stabilize the bonding character, resulting in poor sensitivity in bio- or electrochemical sensor designs (Malhotra and Ali 2018; Hatakeyama et al. 2017). However, GO can be incorporated with composite materials, enhancing tensility, elasticity and impact strength. GO's capability for chemical modification allows diverse bio-medical applications (Novoselov et al. 2012). Thus, erGO has been found to possess a higher charge-transfer characteristic that is not hindered by resistances that occur due to the presence of oxygen bearing groups on the graphenic carbon lattice. erGO exhibits excellent electrochemical characteristics that are far superior to GO and is well-suited for use as an immobilization platform or molecular recognizant for non-enzymatic biosensor (or rather technically, electrochemical sensor) design and drug sensing. GO, by itself, is known for

**Table 4** ECSA,  $J_{WE}$  &  $R_f$  values for erGO/GCE, GO/GCE and GCE determined using EIS data

	erGO/GCE	GO/GCE	GCE
ECSA ( $\text{cm}^2$ )	2.468	1.095	2.374
$R_f$	8.727	3.874	8.395
$J_{WE}$ ( $\mu\text{A}/\text{cm}^2$ )	190.220	30.885	82.436

where 'ECSA' is the electrochemically active surface area, ' $R_f$ ' is roughness factor, and ' $J_{WE}$ ' is exchange current density

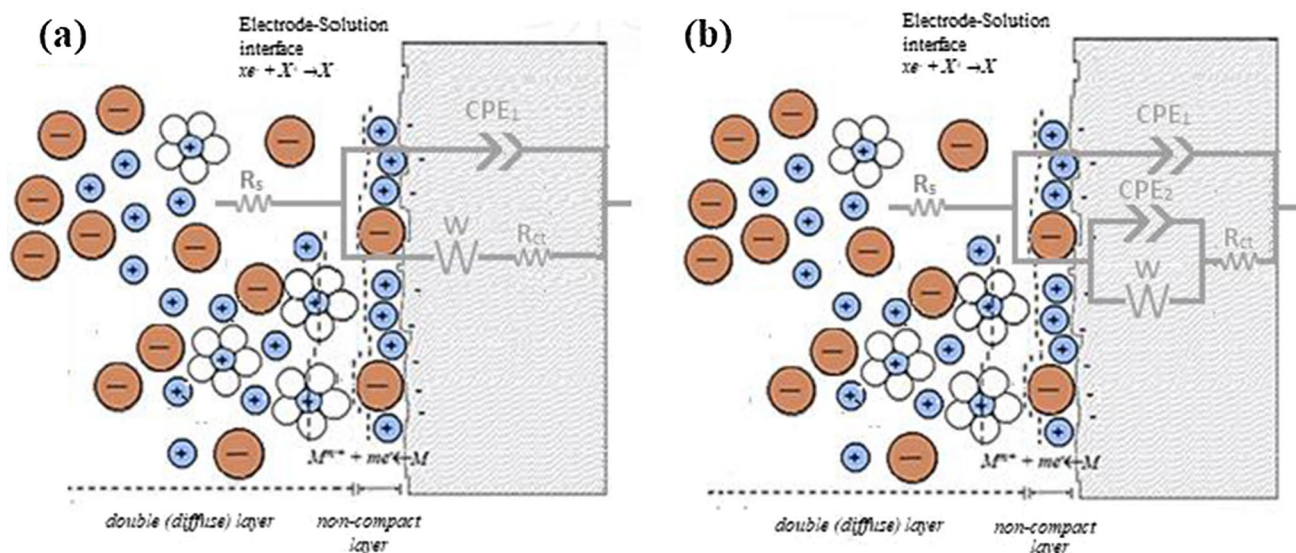


**Fig. 7** Improper diffusion-controlled charge-transfer phenomena between the electrolyte–electrode interface for: **A** diffusion-limited systems i.e. erGO/GCE and bare GCE, and **B** diffusion-controlled

charge-transfer system i.e. GO/GCE. Superimposed are the EECs that give best fit with the phenomena



its poor electrocatalytic activity, unlike its reduced form, erGO (Yu and Kim 2017).

### Electroanalytical probing of GO-based MEs sensing capabilities

#### Differential pulse voltammetric response against Levodopa (LDA) sample

To study the voltammetric behaviour of erGO/GCE electrode, a mixture of LDA, UA and AA was prepared and analysed by differential pulse voltammetry (DPV). DPV curves were recorded at 25 mV/s scan rate using GCE, GO/GCE and erGO/GCE electrodes. erGO/GCE electrode was fabricated at 5 mV/s scan rate, to ensure complete reduction of those oxygen bearing functional groups which possess slow redox behaviour. Figure 8 shows the DPV curves of the GCE, GO/GCE and erGO/GCE electrodes of a mixture of LDA (50  $\mu\text{M}$ ), UA (10  $\mu\text{M}$ ) and AA (1 mM) in 0.1 M PBS (pH 7.0). GCE, GO/GCE and erGO/GCE electrodes show peak corresponding to LDA around 0.2 V (Fig. 8). Measured values are tabulated in Table 5. It can be noted that at about same potential, fabricated erGO/GCE electrode exhibited relatively a well-resolved peak with a considerable higher peak current signal as compared to the GCE and drop-casted GO/GCE electrodes, for the given concentration of LDA in mixture. Furthermore, GCE electrode exhibited only a short peak for LDA at 0.219 V, while not any significant signal was observed for drop-casted GO/GCE electrode, except a somewhat broad response at 0.26 V with a considerably low peak current. This is attributable to the lack of

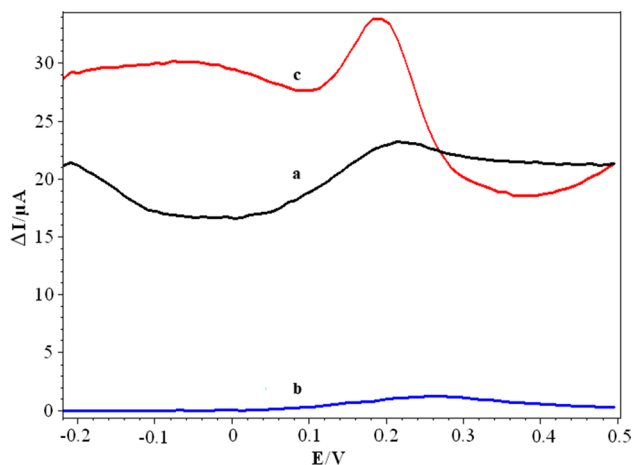


**Fig. 8** Differential pulse voltammogram of 10  $\mu\text{M}$  UA, 50  $\mu\text{M}$  LDA & 1 mM AA mixture in 0.1 M PBS (pH 7.0), from  $-0.200$  V to  $0.500$  V, at 25 mV/s, using **a** GCE, **b** GO/GCE and **c** erGO/GCE

**Table 5** DPV peak values of LDA in a mixture of 50  $\mu\text{M}$  LDA, 10  $\mu\text{M}$  UA and 1 mM AA in 0.1 M APBS (pH 7.0), at 25 mV/s scan rate, using bare GCE, GO/GCE and erGO/GCE electrode

Working electrode	LDA	
	Current/ $\mu\text{A}$	Potential/V
(a) GCE	23.28	0.219
(b) GO/GCE	0.15	0.26
(c) erGO/GCE	33.87	0.20

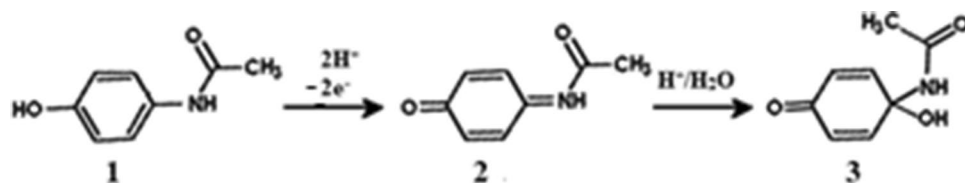
electrocatalytic effects of the GO due to the high resistances offered by the probable high oxidation degree of GO (Yu and Kim 2017; Yan Q. et al. 2020). Thicker films also exhibit high resistivity (see Sect. 3.4.2.) which lead to decrease the sensing effects. As erGO/GCE electrode was fabricated by electrochemical reduction which results in the formation of thin and smooth film on electrode surface and increases its surface area that is why erGO/GCE electrode exhibited well-resolved peak of LDA and could be used efficiently in the presence of UA and AA. Qualitative comparisons of electrocatalytic performances of GO/GCE and erGO/GCE are further explored in Sect. 3.5.2.

A small hump of AA can be seen at  $-0.19$  V on curve ‘a’ of Fig. 8, and this hump was not appeared for curve ‘b’ and also not visible for curve ‘c’. However, a very broad peak may be seen at curve ‘c’ at the potential of interest. This may be due to the lower concentration of that analyte in this mixture. It means GCE electrode was somehow able to detect AA, whereas GO/GCE was completely failed to detect this analyte. The weak response of erGO/GCE electrode towards UA or AA might be due to the high selectivity of our fabricated erGO/GCE electrochemical sensor towards LDA. Stable bonding may exist in between LDA and different functional groups such as LDA-COO and/or LDA-OH and/or H-bonding. Along with this electrostatic type of interactions of the erGO/GCE may also exist in the aqueous neutral buffer. Figure 9 shows the pictorial illustration of proposed LDA-erGO/GCE interaction.

#### Against acetaminophen (APAP) tablet samples

**Acetaminophen (APAP) Electrochemistry:** In an acidic  $\text{pH} \leq 2.0$ , the oxidation of APAP (1) yields the hepatotoxic metabolite N-acetyl-p-benzoquinone imine (NAPQI) (2), which further converts to the electrochemically inactive hydrate (APAP-OH) (3), which cannot be electrochemically reduced back to APAP. The formation of APAP-OH is an irreversible process. The reaction is given as under:





Hence, the cathodic sweep of the CV in Fig. 10A–B illustrates no response. The presence of a significant amount of acidic catalyst further prevents the reduction of the APAP-OH to APAP. However, the electrochemical process changes to quasi-reversible as the pH increases (Van Beschoten et al. 1983; Selvam et al 2020).

**Electrochemical Behaviours with APAP sample:** Cyclic voltammograms of 20 mg/mL APAP in 0.1 M HCl (pH 1.0) were recorded using a triad of WEs, namely: (i) erGO/GCE, (ii) GO/GCE and (iii) bare GCE, to compare electrochemical behaviours and performances of these electrodes. The fabricated erGO/GCE was found to exhibit a well-resolved peak at 0.85 V, with a significantly high anodic response of 163.5  $\mu\text{A}$  at 30 mV/s scan rate and 159.7  $\mu\text{A}$  at 50 mV/s scan rate. By contrast, bare GCE showed relatively lower anodic responses at the two scan rates, while the GO/GCE showed a diminished response, owing to its greater degree of oxidation, stabilization, non-uniform

deposition and thus lower electrocatalytic surface area (Fig. 10 and Table 6). It is also evident from Fig. 10B that at faster scan rates comparatively low peak current was observed, which shows slow kinetics of the conversion of APAP into NAPQI. These results imply that APAP drug can be analysed quantitatively.

**erGO Electrocatalysis on APAP Oxidation:** We illustrate the interaction between erGO/GCE and APAP, as shown in Fig. 10C. The higher electrocatalytic properties drastically improve current responses for the fabricated erGO/GCE, where the oxygen-bearing groups facilitate steady electron transfer to assist oxidation and partial reduction at the low pH.

**Sensing Capability, Detection & Quantification of APAP by Differential Pulse Voltammetry (DPV):** Generic APAP tablets are manufactured globally on an unprecedented scale; thus, a simple, robust sensor is needed for QC and bioavailability testing. The APAP sensing capabilities of erGO/GCE

**Fig. 9** Proposed LDA-erGO/GCE interaction

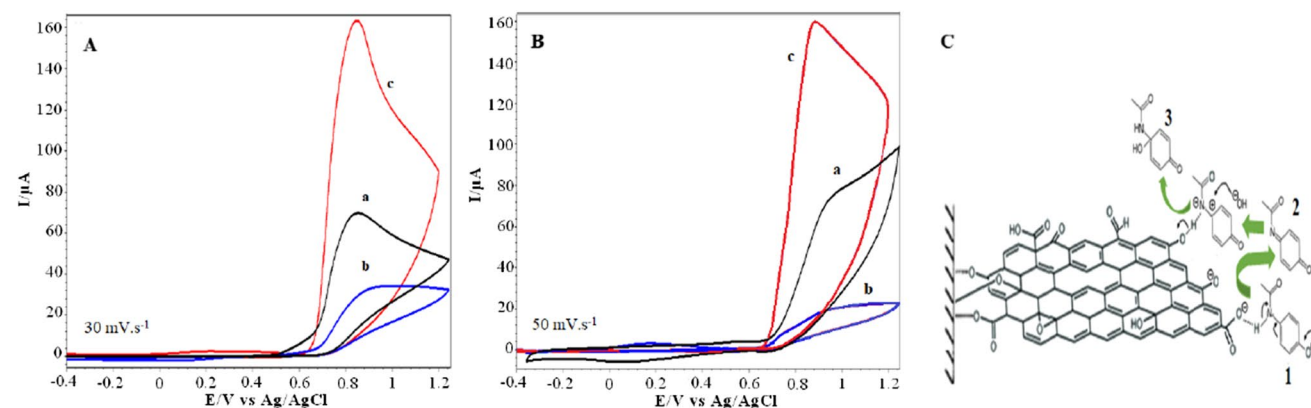
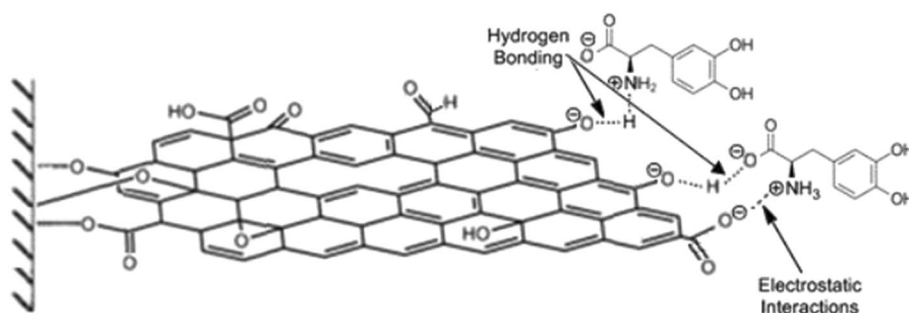


**Fig. 10** Cyclic voltammograms of 0.1 M (20 mg/mL) APAP in 0.1 M HCl (pH 1.0), measured from 0.0 to 1.2 V at **A** 30 mV/s and **B** 50 mV/s; for (a) bare GCE, (b) GO/GCE and (c) fabricated erGO/GCE. **C** Proposed erGO/GCE-assisted electro-catalysed APAP oxidation

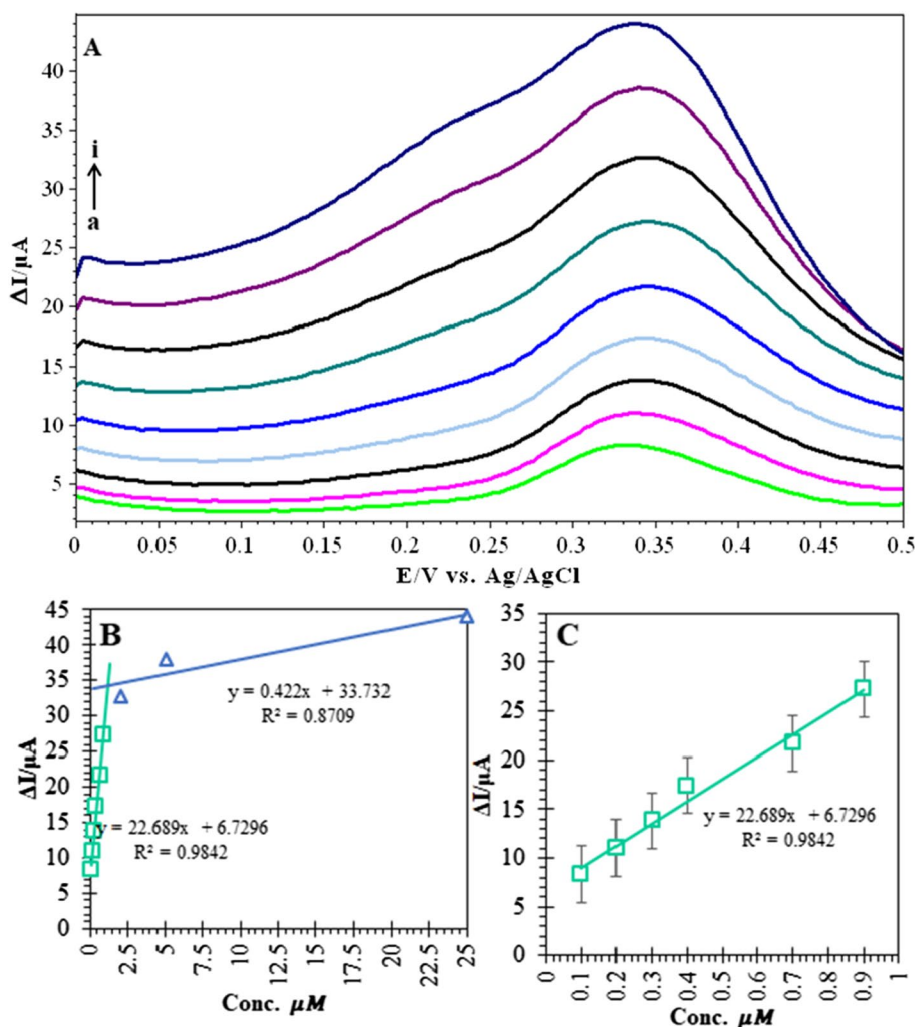
**Table 6** CV measurements of 0.1 M (20 mg/mL) APAP in 0.1 M HCl (pH 1.0) for the (i) fabricated erGO/GCE, (ii) drop-casted GO/GCE and (iii) bare GCE, recorded at  $-0.4$  to  $1.2$  V potential window at varying scan rates (only anodic response observed)

#	Working electrode	At, 30 mV/s		At, 50 mV/s	
		$V_{p,a}/V$	$i_{p,a}/\mu A$	$V_{p,a}/V$	$i_{p,a}/\mu A$
(i)	erGO/GCE	0.85	163.5	0.89	159.7
(ii)	GCE	0.86	109.8	0.89	67.6
(iii)	GO/GCE	0.85	69.1	0.88	18.8

were probed via DPV in the potential range of 0.0 to 0.5 V, at  $8.0 \text{ mV}\cdot\text{s}^{-1}$  scan rate. Figure 11A shows the DPV curves of the erGO/GCE ME under various APAP concentrations (0.1–23  $\mu\text{M}$ ) in 0.1 M HCl (pH 1.0). A single well-defined oxidation peak corresponding to APAP was appeared at 0.340 V. The shoulder observed between 0.17 and 0.27 V range which can be attributed to the initial adsorption of acetaminophen prior to the electrochemical oxidation on the ME surface. Two

sets of calibration curves ( $i_{p,a}$  vs.  $C_{\text{APAP}}$ ), shown in Fig. 11B, were plotted corresponding the lower concentration range, i.e. 0.1–0.9  $\mu\text{M}$  (where sensitivity is maximum), and the higher concentration range, i.e. 2.3–23  $\mu\text{M}$  (beyond working range). The former curve is to be considered for the LOD, LOQ and sensitivity estimation for the erGO/GCE response. Figure 11C shows the DPV calibration plot, indicating the anodic current responses of the erGO/GCE versus varying APAP concentrations. A ‘good’ linear regression was obtained for this calibration plot ( $R^2 = 0.9842$ ). The limit of detection (LOD) and limit of quantification for APAP concentrations were estimated to be 7.23 nM and 21.91 nM. The LOD and LOQ have been estimated using the  $3\sigma$  approach ( $3:1 S/N$  ratio) using Eq. 8 and Eq. 9, respectively, where ‘ $SD_{yx}$ ’ is the standard deviation of the y-residuals and ‘b’ is the slope of the calibration curve. Using  $SD_{yx}$  in LOD and LOQ quantification can lead to better estimate of mean blank signals (Miller 2005; Uhrovčík, 2014).

**Fig. 11** **A** Differential Pulse Voltammogram recorded at 0.0–0.5 V potential range, at  $8 \text{ mV/s}$  scan rate using erGO/GCE with APAP concentrations: (a) 0.1, (b) 0.2, (c) 0.3, (d) 0.4, (e) 0.7, (f) 0.9, (g) 2.3, (h) 4.7 and (i) 23  $\mu\text{M}$ ; in 0.1 M HCl (pH 1.0). **B** Calibration curves ( $i_{p,a}$  vs.  $C_{\text{APAP}}$ ) corresponding to: narrow range (i.e. 0.1–0.9  $\mu\text{M}$ ; teal squares) and **C** broad range (i.e. 2.3–23  $\mu\text{M}$ ; blue triangles)



$$\text{LOD } (\mu\text{M}) = 3.3 \frac{\text{SD}_{yx}}{b}; \quad (8)$$

$$\text{LOQ } (\mu\text{M}) = 10 \frac{\text{SD}_{yx}}{b}; \quad (9)$$

Obtained LOD for APAP was comparable and even improved over previous studies, as presented in Table 7. For QC testing of APAP pharmaceutical formulations, the requisite measurable detection limit (MDL, equiv. to LOD) is  $< 5 \mu\text{M}$ . Thus, the erGO/GCE fabricated in this work can serve as a useful tool for said analysis. APAP oxidation to NAPQI is entirely an irreversible reaction at pH 1.0; thus, its intermediate may not be accumulated at the ME surface. The rapid erGO/GCE-APAP interactions at the electrode surface significantly enhance the electron transfer rate, thereby giving well-defined, linear and highly sensitive responses. The linearity of the DPV response of the erGO/GCE was determined to be 21.91 nM (LOQ) to 2.3  $\mu\text{M}$  (LOL), i.e.: 21.91 nM–2.3  $\mu\text{M}$ . The sensitivity per active surface area for erGO/GCE (ECSA: 2.468  $\text{cm}^2$ ) was found to be 20.142  $\mu\text{A}\cdot\text{nM}^{-1}\cdot\text{cm}^{-2}$ . The current response was observed to be linearly changed with the increase in APAP concentrations. The detection range obtained in this study might be used for the evaluation of orally administered APAP. The average plasma concentration of APAP (500 mg) through oral administration after 28.5 h is 2.3  $\mu\text{M}$ , respectively (Rawlins et al 1977; Hoffman et al 2015).

Thus, the DPV linear range (21.91 nM to 2.3  $\mu\text{M}$ ) for the erGO/GCE may be used for the evaluation of probable hepatotoxic onsets after ingestion. The fabricated erGO/GCE

electrochemical sensor was used at least 5–8 runs per technique beyond which the signal-to-noise ratio becomes significantly low as the thin-film erodes away in the aqueous media.

*Studying APAP electrocatalytic oxidation by erGO/GCE using Chronoamperometry (CAmp)*: The APAP electrocatalytic oxidation by the erGO/GCE was further studied by chronoamperometry. Chronoamperogram as shown in Fig. 12A is recorded for the erGO/GCE ME under various concentrations of APAP (0.1, 0.2, 0.4, 0.5, 0.7, 0.9  $\mu\text{M}$ ) in 0.1 M HCl (pH 1.0).

The effect of the applied electrode potential of 0.34 V (APAP oxidation potential) indicated that the anodic current response rapidly increases with increasing concentrations of APAP. APAP diffusion coefficient (D) can be evaluated by using the Cottrell equation, Eq. 10 (Bard 2001):

$$i = nFAC_{\text{APAP}} \sqrt{\frac{D}{\pi t}}; \quad (10)$$

where ‘D’ is the diffusion coefficient ( $\text{cm}^2\cdot\text{s}^{-1}$ ), ‘ $C_{\text{APAP}}$ ’ is the APAP concentration ( $\text{mol}\cdot\text{cm}^{-3}$ ), ‘A’ is ECSA (2.468  $\text{cm}^2$ ), ‘F’ is the Faraday’s constant (96,485  $\text{C}\cdot\text{mol}^{-1}$ ), and ‘n’ is the number of electrons transferred (2 electrons). The experimental plots of  $i$  vs.  $t^{-1/2}$  with the best fit for different  $C_{\text{APAP}}$  were used, as shown in Fig. 12B. Resulting slopes were plotted against  $C_{\text{APAP}}$ , as shown in Fig. 12C. It shows a relatively good linear relationship in the tested APAP concentration range, with a correlation coefficient of  $R^2=0.8846$ . From the slope of this plot, the ‘D’ APAP was calculated as  $2.24 \times 10^{-5} \text{cm}^2\cdot\text{s}^{-1}$ . The ‘D’ value is similar in

**Table 7** Comparison of detection limits for APAP by various techniques

Methods	Specification	Linearity ( $\mu\text{M}$ )	LOD ( $\mu\text{M}$ )	Ref.
HPLC		33.11–397.35	0.199	Calinescu et al. (2012)
Colorimetry			400,000	Shihana et al. (2010)
Chemi luminescence		0.025–0.25	0.01	Easwaramoorthy et al. (2001)
CA	Gr/PDDA/PSS-fMWCNT	25–400	0.5	Manjunathaa et al. (2011)
DPV	$\text{Fe}_3\text{O}_4$ -PDDA-Gr/GCE		0.037	Lu et al. (2012)
DPV	erGO/ $\text{Ni}_2\text{O}_3$ -NiO/GCE	0.04–100	0.02	Liu G.T. et al. (2014)
SWV	Gr modified GCE		0.038	Kang et al. (2010)
DPV	Nafion/ $\text{TiO}_2$ -Gr/GCE	1–20	0.21	Fan et al. (2011)
DPV	NC-GPE		3.71	Patil et al. (2019)
DPV	$\text{C}_{60}$ /GCE	0.05–1500	50.0	Goyal et al. (2006)
DPV	SWCNT-Gr/GCE	0.05–64.5	0.038	Chen X. et al. (2012)
DPV	MWCNTs-NHNPs/GCE	0.06–26	0.017	Babaei et al. (2013)
DPV	erGO/GCE	0.0022–2.3	0.00724	Present work

$\text{C}_{60}$  buckyball/fullerene; erGO electrochemically reduced graphene oxide; Gr grapheme; GPE graphite paste electrode; GCE glassy carbon electrode; fMWCNT functionalized multi-walled carbon nanotubes; NC nanoclay; PDDA poly(diallyldimethylammonium chloride); PSS polystyrene sulfonate; SWCNT single-walled carbon nanotubes

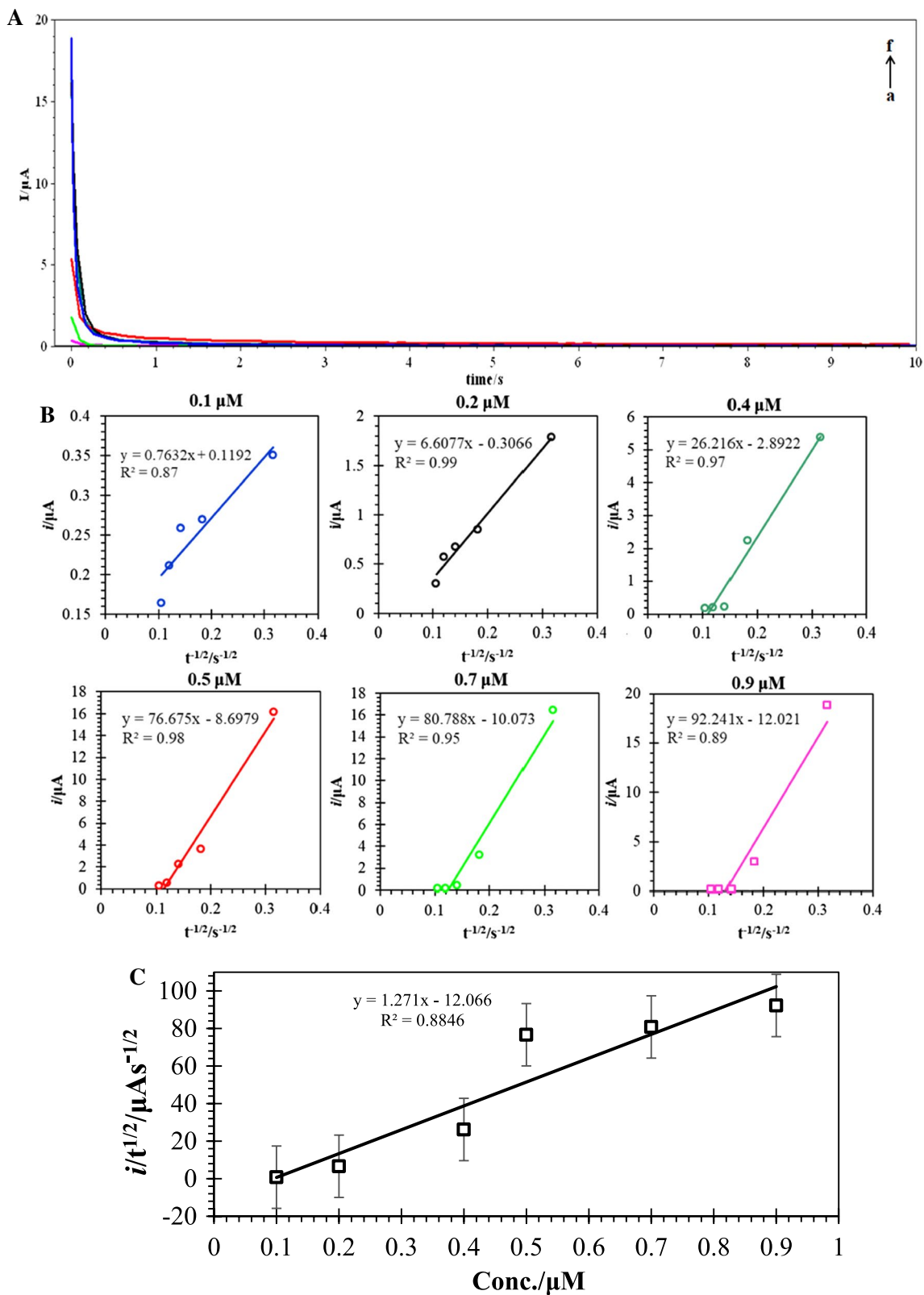


**Fig. 12** **A** Chronoamperogram of varying APAP concentrations: (a) 0.1  $\mu\text{M}$ , (b) 0.2  $\mu\text{M}$ , (c) 0.4  $\mu\text{M}$ , (d) 0.5  $\mu\text{M}$ , (e) 0.7  $\mu\text{M}$  and (f) 0.9  $\mu\text{M}$ ; in 0.1 M HCl (pH 1.0), using erGO/GCE. CAmp performed

at 0.34 V, at 10 s. **B**  $i$  vs.  $t^{-1/2}$  curves for varying APAP concentrations. **C** Ultimate slope curve: resulting slopes vs. APAP concentrations plot

terms of its exponent to that reported for APAP in aqueous media ( $10^{-9} \text{ m}^2 \cdot \text{s}^{-1}$ ) (Ribiero et al. 2012).

### Eco-scale and analytical eco-scale assessment

The green character of our proposed sensor was evaluated by the Eco-Scale (DeVierno Kreuder et al 2017) and Analytical Eco-Scale (Sajid et al. 2022) approach. These intuitive post-syntheses and post-analyses tools assign cumulative scores after evaluating the given method against the parameter-penalty tables, Table S1 and Table S2 (see Supplementary Information), where the associated risks, hazards and negative impacts of the method parameters are under consideration. These penalties are subtracted from the maximum score (100) representing an ideal ‘green’ reaction to get a value that ranks the synthetic methods in terms of its green quality (for high-purity products). Details of penalty calculations for the improved GO synthesis are given in Table S3 (see Supplementary Information), whereas penalty calculations for erGO/GCE ME fabrication, electrochemical performance evaluation and for APAP voltammetric assays, are given in Table S4 (see Supplementary Information). The estimated values for both assessment approaches can be ranked on a 0–100 greenness scale against the following criteria: > 75, excellent; > 50, acceptable; and < 50, inadequate. The synthetic method as proposed in the present work was assessed using the Eco-scale approach, giving a 66 score (acceptable), while the overall electro-reductive fabrication and electroanalytical procedures performed, giving a 93 score (excellent).

### Conclusion

This study presents a facile, rapid, eco-friendly, sensitive and accurate electrochemical biosensor for acetaminophen (APAP) determination in pharmaceutical formulations. In this study, we design erGO nanosheets as electrochemical biosensor using an optimized LSV electrochemical technique. Characterization results of GO nanosheets have been obtained using UV–Vis, XRD, FE-SEM and FTIR techniques, which were found compliant with the literature. Our nanomaterial possesses distinct morphology and unique crystallite having dimension  $26.5 \text{ nm} \times 5.5 \text{ nm}$  with 0.86-nm layer separation. CV & EIS techniques have been used to evaluate electrochemical performance of the bare GCE, drop-casted GO/GCE and erGO/GCE. erGO/GCE performance was found much better than other substrates. erGO/GCE sensor was found to exhibit thin-film uniformity, higher surface activities and enhanced electrocatalysis. We also demonstrated the use of a novel FTIR-ATR characterization technique for the surface modification of the LSV-fabricated non-enzymatic erGO/GCE electrochemical sensor, allowing for rapid, simple and reliable surface modification analysis

in comparison of FE-SEM or Raman techniques. Further to that relatively high anodic current responses were recorded by DPV measurements for the APAP tablet samples in micro molar concentration ranges using erGO/GCE sensor. A linearity of 21.91 nM–2.3  $\mu\text{M}$  was observed. The LOD, LOQ and sensitivity per active surface area for the erGO/GCE with APAP were found to be 7.23 nM, 21.91 nM and  $20.142 \mu\text{A} \cdot \text{nM}^{-1} \cdot \text{cm}^{-2}$ , respectively. A diffusion coefficient of  $2.24 \times 10^{-5} \text{ cm}^2 \cdot \text{s}^{-1}$  was also determined using chronoamperometry. Based on these results it may be concluded that the fabricated erGO/GCE electrochemical sensor could be used for QC testing and APAP post-ingestion hepatotoxic studies. The Eco-Scale & Analytical Eco-Scale assessment tools provided a 66 score (acceptable) for the synthetic procedure and a 93 score (excellent) for the overall electroanalytical assays (including electro-reductive fabrication for erGO/GCE ME) performed in this study.

**Supplementary Information** The online version contains supplementary material available at <https://doi.org/10.1007/s11696-022-02628-9>.

**Acknowledgements** Authors would like to acknowledge the technical assistance provided by the Department of Material Sciences (NED University of Engineering & Technology, Karachi, Pakistan), Department of Applied Physics (NED University of Engineering & Technology, Karachi, Pakistan) and the LEJ Nanotechnology Center, ICCBS (Karachi, Pakistan).

**Funding** This research did not receive any specific grant from funding agencies in the public, commercial or not-for-profit sectors.

**Data availability** All data generated or analysed during this study are included in this published article (and its supplementary information files).

### Declarations

**Conflict of interest** The authors declare that there is no conflict of interests regarding the publication of this paper.

### References

- Ahmad J (2011) Hepatology and transplant hepatology: a case based approach, Cases 1–26. In: Hepatology and Transplant Hepatology. Springer, Boston, MA. [https://doi.org/10.1007/978-1-4419-7085-5\\_1](https://doi.org/10.1007/978-1-4419-7085-5_1)
- Ahmad K, Mohammad A, Ansari SN, Mobin SM (2018) Construction of graphene oxide sheets based modified glassy carbon electrode (GO/GCE) for the highly sensitive detection of nitrobenzene. Mater Res Express 5:075601. <https://doi.org/10.1088/2053-1591/aacd98>
- Babaei A, Sohrabi M, Taheri AR (2013) Highly sensitive simultaneous determination of l-dopa and paracetamol using a glassy carbon electrode modified with a composite of nickel hydroxide nanoparticles/multi-walled carbon nanotubes. J Electroanal 698:45–51. <https://doi.org/10.1016/j.jelechem.2013.01.021>
- Bard AJ, Faulkner LR (2001) Electrochemical methods: fundamentals and applications, 2nd edn. Wiley, New York




- Bessemers JG, Vermeulen NP (2001) Paracetamol (acetaminophen)-induced toxicity: molecular and biochemical mechanisms, analogues and protective approaches. *Crit Rev Toxicol* 31:55–138. <https://doi.org/10.1080/20014091111677>
- Benschoten V, James J, Lewis JY, Heineman WR, Roston DA, Kissinger PT (1983) Cyclic voltammetry experiment. *J Chem Ed* 60(9):772. <https://doi.org/10.1021/ed060p772>
- Burgot G, Auffret F, Burgot JL (1997) Determination of acetaminophen by thermometric titrimetry. *Anal Chem Acta* 343:125–128. [https://doi.org/10.1016/S0003-2670\(96\)00613-7](https://doi.org/10.1016/S0003-2670(96)00613-7)
- Calinescu O, Badea IA, Vladescu L, Meltzer V, Pincu E (2012) HPLC separation of acetaminophen and its impurities using a mixed-mode reversed-phase/cation exchange stationary phase. *J Chromatogr Sci* 50(4):335–342. <https://doi.org/10.1093/chromsci/bmr043>
- Casero E, Parra-Alfambra AM, Petit-Domínguez MD, Pariente F, Lorenzo E, Alonso C (2012) Differentiation between graphene oxide and reduced graphene by electrochemical impedance spectroscopy (EIS). *Electrochem Commun* 20:63–66. <https://doi.org/10.1016/j.elecom.2012.04.002>
- Connor W, Schuch J, Kaiser B, Jaegermann W (2020) The determination of electrochemical active surface area and specific capacity revisited for the system MnOx as an oxygen evolution catalyst. *Z Phys Chem* 234(5):979–994. <https://doi.org/10.1515/zpch-2019-1514>
- Chen A, Chatterjee S (2013) Nanomaterials based electrochemical sensors for biomedical applications. *Chem Soc Rev* 42:5425–5438. <https://doi.org/10.1039/C3CS35518G>
- Chen J, Yao B, Li C, Shi G (2013) An improved Hummers method for eco-friendly synthesis of graphene oxide. *Carbon* 64:225–229. <https://doi.org/10.1016/j.carbon.2013.07.055>
- Chen X, Zhu J, Xi Q, Yang W (2012) A high performance electrochemical sensor for acetaminophen based on single-walled carbon nanotube–graphene nanosheet hybrid films. *Sens Actuators B Chem* 161(1):648–654. <https://doi.org/10.1016/j.snb.2011.10.085>
- Cui D, Gao A, Liang H, Tian J, Li X, Shen Q (2020) Nano coronavirus recombinant vaccine taking graphene oxide as carrier. *PRC Patent No.* CN112220919A
- DeVierno Kreuder A, House-Knight T, Whitford J, Ponnusamy E, Miller P, Jesse N, Rodenborn R, Sayag S, Gebel M, Aped I, Sharfstein I, Manaster E, Ergaz I, Harris A, Nelowet Grice L (2017) A method for assessing greener alternatives between chemical products following the 12 principles of green chemistry. *ACS Sustain Chem Eng* 5:2927–2935. <https://doi.org/10.1021/acssu.chemeng.6b02399>
- Dorset DL (1998) X-ray diffraction: a practical approach. *Microsc Microanal* 4(5):513–515. <https://doi.org/10.1017/s143192769800049x>
- Easwaramoorthy D, Yu YC, Huang HJ (2001) Chemiluminescence detection of paracetamol by a luminol-permanganate based reaction. *Anal Chim Acta* 439:95–100. [https://doi.org/10.1016/S0003-2670\(01\)00968-0](https://doi.org/10.1016/S0003-2670(01)00968-0)
- Eigler S, Dimiev AM (2016) Characterization techniques. *Graphene oxide*. John Wiley & Sons Ltd, New York, pp 85–120
- Eigler S, Hirsch A (2012) Preparation method for graphene oxide suitable for graphene production. *Eur Pat No.* 2639201A1
- Fan Y, Liu JH, Lu HT, Zhang Q (2011) Electrochemical behavior and voltammetric determination of paracetamol on Nafion/TiO<sub>2</sub>-graphene modified glassy carbon electrode. *Colloids Surf B* 85:289–292. <https://doi.org/10.1016/j.colsurfb.2011.02.041>
- Fujino H, Yoshida H, Nohta H, Yamaguchi M (2005) HPLC determination of acetaminophen in saliva based on precolumn fluorescence derivatization with 12-(3,5-Dichloro-2,4,6-Triazinyl) Benzo[d] Benzo[1',2'-6,5]Isoindolo[1, 2-b][1,3]Thiazolidine. *Anal Sci* 21:1121–1124. <https://doi.org/10.2116/analsci.21.1121>
- Gałuszka A, Migaszewski ZM, Konieczka P, Namieśnik J (2012) Analytical eco-scale for assessing the greenness of analytical procedures. *TrAC* 37:61–72. <https://doi.org/10.1016/j.trac.2012.03.013>
- Goyal RN, Singh SP (2006) Voltammetric determination of paracetamol at C60-modified glassy carbon electrode. *Electrochim Acta* 51(15):3008–3012. <https://doi.org/10.1016/j.electacta.2005.08.036>
- Graphene Oxide Analysis (GOgraphene). <https://www.go-graphene.com/pages/graphene-oxide-analysis>. Accessed Apr 29, 2022
- Harris PJF (2004) Fullerene-related structure of commercial glassy carbons. *Philo Mag Lett* 84(29):3159–3167. <https://doi.org/10.1080/14786430410001720363>
- Hatakeyama K, Hayami S, Matsumoto Y (2017) Graphene oxide based electrochemical system for energy generation. In: Nakato T, Kawamata J, Takagi S (eds) *Inorganic nano-sheets and nanosheet-based materials*. Nanostructure science and technology. Springer, Tokyo
- Hidayah NMS, Liu WW, Lai CW, Noriman NZ, Khe CS, Hashim U, Lee HC (2017) Comparison on graphite, graphene oxide and reduced graphene oxide: synthesis and characterization. *AIP Conf Proc* 1892(1):150002. <https://doi.org/10.1063/1.5005764>
- Hoffman RS, Howland M, Lewin NA, Nelson LS, Goldfrank LR (2015) *Goldfrank's Toxicologic Emergencies*, 10e, Acetaminophen. <https://accessemergencymedicine.mhmedical.com/content.aspx?bookid=1163&sectionid=65093210>. Accessed Mar 15, 2022
- Hummerts WS Jr, Offeman RE (1958) Preparation of graphitic oxide. *J Am Chem Soc* 80:1339–1339. <https://doi.org/10.1021/ja01539a017>
- James LP, Mayeux PR, Hinson JA (2003) Acetaminophen-induced hepatotoxicity. *Drug metabolism and disposition: the biological fate of chemicals*. *Drug Metab* 31(12):1499–1506. <https://doi.org/10.1124/dmd.31.12.1499>
- Kang X, Wang J, Wu H, Liu J, Aksay IA, Lin Y (2010) A graphene-based electrochemical sensor for sensitive detection of paracetamol. *Talanta* 81:754–759. <https://doi.org/10.1016/j.talanta.2010.01.009>
- Khan QA, Shaur A, Khan TA, Joya YF, Awan MS (2017) Characterization of reduced graphene oxide produced through a modified Hoffman method. *Cogent Chem* 3(1):1298980. <https://doi.org/10.1080/23312009.2017.1298980>
- Kumar KG, Letha R (1997) Determination of paracetamol in pure form and in dosage forms using N, N-dibromo dimethylhydantoin. *J Pharm Biomed* 15(11):1725–1728. [https://doi.org/10.1016/s0731-7085\(96\)01976-0](https://doi.org/10.1016/s0731-7085(96)01976-0)
- Liu GT, Chen HF, Lin GM, Ye PP, Wang XP, Jiao YZ, Guo XY, Wen Y, Yang HF (2014) One-step electrodeposition of graphene loaded nickel oxides nanoparticles for acetaminophen detection. *Biosens Bioelectron* 56:26–32. <https://doi.org/10.1016/j.bios.2014.01.005>
- Liu J, Cui L, Losic D (2013) Graphene and graphene oxide as new nanocarriers for drug delivery applications. *Acta Biomater* 9(12):9243–9257. <https://doi.org/10.1016/j.actbio.2013.08.016>
- Low FW, Lai CW, Abd Hamid SB (2015) Easy preparation of ultrathin reduced graphene oxide sheets at a high stirring speed. *Ceram Int* 41(4):5798–5806. <https://doi.org/10.1016/j.ceramint.2015.01.008>
- Lu D, Zhang Y, Wang L, Lin S, Wang C, Chen X (2012) Sensitive detection of acetaminophen based on Fe<sub>3</sub>O<sub>4</sub> nanoparticles-coated poly(diallyldimethylammonium chloride)-functionalized graphene nanocomposite film. *Talanta* 88:181–186. <https://doi.org/10.1016/j.talanta.2011.10.029>
- Malhotra BD, Ali MA (2018) Nanomaterials in Biosensors. *Nanomater Biosens*. <https://doi.org/10.1016/B978-0-323-44923-6.00001-7>
- Manjunathaa R, Nagarajub DH, Suresha GS, Meloc JS, D'souza SF, Venkateshad TV (2011) Electrochemical detection of acetaminophen on the functionalized MWCNTs modified electrode using layer-by-layer technique. *Electrochim Acta* 56:6619–6627. <https://doi.org/10.1016/j.electacta.2011.05.018>

- Marcano DC, Kosynkin DV, Berlin JM, Sinitzskii A, Sun Z, Slesarev A, Alemany LB, Lu W, Tour JM (2010) Improved synthesis of graphene oxide. *ACS Nano* 4(8):4806–4814. <https://doi.org/10.1021/nn1006368>
- Miller JN, Miller JCh (2005) *Statistics and chemometrics for analytical chemistry*, 5th edn. Ellison Horwood, Chichester
- Moreira AB, Oliveira HPM, Atvars TDZ, Dias LLT, Neto GO, Zagatto EAG, Kubota LT (2005) Direct determination of paracetamol in powdered pharmaceutical samples by fluorescence spectroscopy. *Anal Chem Acta* 539:257–261. <https://doi.org/10.1016/j.aca.2005.03.012>
- Mudunkotuwa IA, Minshid AA, Grassian VH (2014) ATR-FTIR spectroscopy as a tool to probe surface adsorption on nanoparticles at the liquid–solid interface in environmentally and biologically relevant media. *Analyst* 139:870–881. <https://doi.org/10.1039/c3an01684f>
- Nagaraja P, Srinivasa Murthy KC, Rangappa KS (1998) Spectrophotometric method for the determination of paracetamol and phenacetin. *J Pharm Biomed* 17(3):501–506. [https://doi.org/10.1016/S0731-7085\(97\)00237-9](https://doi.org/10.1016/S0731-7085(97)00237-9)
- Novoselov KS, Fal'Ko VI, Colombo L, Gellert PR, Schwab MG, Kim K (2012) A roadmap for graphene. *Nature* 490(7419):192–200. <https://doi.org/10.1038/nature11458>
- Pareek A, Shanthi Sravan J, Venkata Mohan S (2019) Graphene modified electrodes for bioelectricity generation in mediator-less microbial fuel cell. *J Mat Sci* 54(17):11604–11617. <https://doi.org/10.1007/s10853-019-03718-y>
- Patil MM, Shetti NP, Malode SJ, Nayak DS, Chakklabbi TR (2019) Electroanalysis of paracetamol at nanoclay modified graphite electrode. *Mater* 18:986–993. <https://doi.org/10.1016/j.matpr.2019.06.538>
- Popova AN (2017) Crystallographic analysis of graphite by X-Ray diffraction. *Coke Chem* 60(9):361–365. <https://doi.org/10.3103/S1068364X17090058>
- Ravisankar S, Vasudevan M, Ganhimathi M, Suresh B (1998) Reversed-phase HPLC method for the estimation of acetaminophen, ibuprofen and chlorzoxazone in formulations. *Talanta* 46:1577–1581. [https://doi.org/10.1016/S0039-9140\(98\)00043-5](https://doi.org/10.1016/S0039-9140(98)00043-5)
- Rawlins MD, Henderson DB, Hijab AR (1977) Pharmacokinetics of paracetamol (acetaminophen) after intravenous and oral administration. *Eur J Clin Pharmacol* 11:283–286. <https://doi.org/10.1007/BF00607678>
- Ribeiro ACF, Barros MCF, Veríssimo LMP, Santos CIAV, Cabral AMTDPV, Gaspar GD, Esteso MA (2012) Diffusion coefficients of paracetamol in aqueous solutions. *J Chem Thermodyn* 54:97–99. <https://doi.org/10.1016/j.jct.2012.03.014>
- Roy S, Soin N, Bajpai R, Misra DS, McLaughlin JA, Roy SS (2011) Graphene oxide for electrochemical sensing applications. *J Mater Chem* 21(38):14725. <https://doi.org/10.1039/C1JM12028J>
- Sajid M, Plotka-Wasyłka J (2022) Green analytical chemistry metrics: a review. *Talanta* 238:123046. <https://doi.org/10.1016/j.talanta.2021.123046>
- Senthil RA, Selvi A, Arunachalam P, Amudha LS, Madhavan J, Al-Mayouf AM (2017) A sensitive electrochemical detection of hydroquinone using newly synthesized  $\alpha$ -Fe<sub>2</sub>O<sub>3</sub>-graphene oxide nanocomposite as an electrode material. *J Mater Sci Mater Electron* 28:10081–10091. <https://doi.org/10.1007/s10854-017-6769-x>
- Selvam SP, Chinnadayala SR, Cho S, Yun K (2020) Differential pulse voltammetric electrochemical sensor for the detection of etidronic acid in pharmaceutical samples by using rGO-Ag@SiO<sub>2</sub>/Au PCB. *Nanomaterials* 10(7):1368. <https://doi.org/10.3390/nano10071368>
- Shihana F, Dissanayake D, Dargan P, Dawson A (2010) A modified low-cost colorimetric method for paracetamol (acetaminophen) measurement in plasma. *Clin Toxicol* 48(1):42–46. <https://doi.org/10.3109/15563650903443137>
- Song J, Wang X, Chang CT (2014) Preparation and characterization of graphene oxide. *J Nanomater* 2014:1–6. <https://doi.org/10.1155/2014/276143>
- Stankovich S, Dikin DA, Piner RD, Kohlhaas KA, Kleinhammes A, Jia Y, Ruoff RS (2007) Synthesis of graphene-based nanosheets via chemical reduction of exfoliated graphite oxide. *Carbon* 45(7):1558–1565. <https://doi.org/10.1016/j.carbon.2007.02.034>
- Tsai D-H, Davila-Morris M, DeRio FW, Guha S, Zachariah MR, Hackley VA (2011) Quantitative determination of competitive molecular adsorption on gold nanoparticles using attenuated total reflectance-fourier transform infrared spectroscopy. *Langmuir* 27(15):9302–9313. <https://doi.org/10.1021/LA200542>
- Uhrovčik J (2014) Strategy for determination of LOD and LOQ values—Some basic aspects. *Talanta* 119:178–180. <https://doi.org/10.1016/j.talanta.2013.10.061>
- Van Aken K, Strekowski L, Patiny L (2006) EcoScale, a semi-quantitative tool to select an organic preparation based on economical and ecological parameters. *Beilstein J Org Chem*. <https://doi.org/10.1186/1860-5397-2-3>
- Veerapandian M, Lee MH, Krishnamoorthy K, Yun K (2012) Synthesis, characterization and electrochemical properties of functionalized graphene oxide. *Carbon* 50(11):4228–4238. <https://doi.org/10.1016/j.carbon.2012.05.004>
- Yan Q, Zhi N, Yang L, Xu G, Feng Q, Zhang Q, Sun S (2020) A highly sensitive uric acid electrochemical biosensor based on a nanocube cuprous oxide/ferrocene/uricase modified glassy carbon electrode. *Sci Rep*. <https://doi.org/10.1038/s41598-020-67394-8>
- Yu J, Kim TH (2017) A facile electrochemical fabrication of reduced graphene oxide-modified glassy carbon electrode for simultaneous detection of dopamine, ascorbic acid, and uric acid. *J Electrochem* 8(4):274–281. <https://doi.org/10.5229/JECST.2017.8.4.274>
- Zhang Y, Chung TS (2017) Graphene oxide membranes for nanofiltration. *Curr Opin Chem Eng* 16:9–15. <https://doi.org/10.1016/j.coche.2017.03.002>

**Publisher's Note** Springer Nature remains neutral with regard to jurisdictional claims in published maps and institutional affiliations.

Springer Nature or its licensor (e.g. a society or other partner) holds exclusive rights to this article under a publishing agreement with the author(s) or other rightsholder(s); author self-archiving of the accepted manuscript version of this article is solely governed by the terms of such publishing agreement and applicable law.

## Authors and Affiliations

Muzamil Jalil Ahmed<sup>1</sup> · Shazia Perveen<sup>1</sup>  · Syed Ghazanfar Hussain<sup>1</sup> · Arsalan Ahmed Khan<sup>1</sup> · Syed Muhammad Wahaj Ejaz<sup>1</sup> · Syed Muhammad Ali Rizvi<sup>1</sup>

✉ Shazia Perveen  
shaziaperveen@neduet.edu.pk

<sup>1</sup> Department of Chemistry, NED University of Engineering & Technology, University Road, Karachi, Sindh 75270, Pakistan